Bacterial cGAS senses a viral RNA to initiate immunity

Dalton V. Banh[1,2,#], Cameron G. Roberts[1,#], Adrian Morales Amador[3], Sean F. Brady[3] and Luciano A. Marraffini[1,4*]

[1]Laboratory of Bacteriology, The Rockefeller University, 1230 York Ave, New York, NY 10065, USA.

[2]Weill Cornell/Rockefeller/Sloan Kettering Tri-Institutional MD-PhD Program, 1300 York Ave, New York, NY 10065, USA.

[3]Laboratory of Genetically Encoded Small Molecules, The Rockefeller University, 1230 York Ave, New York, NY 10065, USA.

[4]Howard Hughes Medical Institute, The Rockefeller University, 1230 York Ave, New York, NY 10065, USA.

[#]these authors contributed equally to this study.

*Correspondence to: marraffini@rockefeller.edu

ABSTRACT

CBASS immunity protects prokaryotes from viral (phage) attack through the production of cyclic dinucleotides which activate effector proteins that trigger the death of the infected host. How bacterial cyclases recognize phage infection is not known. Here we show that staphylococcal phages produce a highly structured 400-nt RNA, termed CBASS-activating bacteriophage RNA (cabRNA), that binds to a positively charged surface of the CdnE03 cyclase and promotes the synthesis of the cyclic dinucleotide cGAMP. Phages that escape CBASS immunity harbor mutations that lead to the generation of a longer form of the cabRNA that cannot activate CdnE03. Since the mammalian cyclase OAS1 also binds viral dsRNA during the interferon response, our results reveal a conserved mechanism for the activation of innate antiviral defense pathways.

INTRODUCTION

As a result of an evolutionary arms race, bacteria have evolved numerous immune strategies to counter infection by predatory viruses known as bacteriophages (or phages). Remarkably, many recently discovered antiviral systems in bacteria share structural and functional homology to components of metazoan innate immunity [1,2]. One key example of this ancestral connection includes cyclic oligonucleotide-based antiphage signaling systems (CBASS) in bacteria [3,4], which are analogous to the cyclic GMP-AMP synthase (cGAS)-stimulator of interferon genes (STING) antiviral pathway in metazoans [5,6]. CBASS contain two core components: a cGAS/DncV-like cyclic dinucleotidyltransferase (CD-NTase, or Cdn) enzyme that generates cyclic nucleotides in response to phage infection [7-9], and an effector protein that binds the cyclic nucleotides to trigger the death or growth arrest of the host and thus inhibit viral propagation [3,4,9]. In addition to the cyclase and effector genes, CBASS operons can encode for accessory proteins that are used for their classification into four major types [4]. Type I CBASS comprise the minimal and most abundant architecture (42% of the analyzed operons have this composition). Type II CBASS (39%, the second most common) encode additional genes with ubiquitin-associated domains. Type III CBASS (10%) include regulatory genes that encode eukaryotic-like HORMA and TRIP13 domains [10]. Finally, Type IV CBASS are the rarest and is enriched in archaea [4].

A central aspect of cyclic nucleotide-based immunity is the mechanism of activation of the cyclase; i.e., how the enzyme senses viral infection to begin the synthesis of the second messenger. For human cGAS, this is achieved through direct interaction with viral double-stranded DNA present in the cytosol [6,11-14]. Other cGAS homologs present

in animals, however, can sense RNA instead of DNA [15-18]. In contrast to metazoan cGAS-based immunity, the mechanisms that govern cyclase activation during the bacterial CBASS response are poorly understood. Biochemical analyses of bacterial cyclases from a variety of divergent CBASS operons demonstrated that some of these enzymes are constitutively active *in vitro* [9], suggesting that their activity *in vivo* is negatively regulated and only unleashed upon phage recognition. For instance, it has been proposed that the type II CBASS cyclase DncV from *Vibrio cholerae* is inhibited by folate-like molecules [19]. These metabolites are presumably depleted during infection, a decrease that triggers second messenger production. However, there are also many examples of CBASS cyclases that are inactive *in vitro,* and therefore must require a mechanism of activation to initiate the immune response. This seems to be the case for the *E. coli* type III CBASS, which is activated *in vitro* through recognition of peptides (presumably of phage origin) by HORMA domain proteins that then form a complex with the cognate cyclase to initiate cyclic nucleotide synthesis [10]. Interestingly, this system requires not only the HORMA domain protein, but also the binding of dsDNA by the cyclase for activation *in vitro* [10]. How immunity is initiated by minimal CBASS operons that lack regulatory genes is not known. Here we investigated the mechanism of activation of the cyclase present in the minimal type I CBASS from *Staphylococcus schleiferi.* We found that both *in vitro* and *in vivo*, the binding of a structured RNA produced by staphylococcal phages during infection leads to the synthesis of cGAMP, which in turn activates a transmembrane effector to induce abortive infection.

RESULTS

CBASS protects staphylococci from phage infection.

Bioinformatic analyses have previously uncovered more than 100 CBASS operons in diverse *Staphylococcus* strains [4], none of which, however, have been tested experimentally. We decided to characterize a type I-B CBASS present in *Staphylococcus schleiferi* strains 2142-05, 2317-03, and 5909-02 [20], hereafter designated Ssc-CBASS (Fig. S1A). This system consists of a two-gene operon harboring a Cdn belonging to the E clade, cluster 3 (Ssc-CdnE03) [9], and a transmembrane effector, Cap15, that was recently demonstrated to limit phage propagation by disrupting the host membrane [21]. Since we were unable to find a phage that infects this organism, we cloned Ssc-CBASS, as well as the cyclase gene alone as a control, into the staphylococcal vector pC194 [22] for expression in the laboratory strain *Staphylococcus aureus* RN4220 [23]. The resulting strain was infected with four lytic phages on soft-agar plates to enumerate plaque formation. We found that Ssc-CBASS, but not Ssc-CdnE03 alone, strongly reduced the propagation of Φ80α-vir [a lytic derivative of the temperate phage Φ80α [24] created for this study] and ΦNM1γ6 [25], but not for ΦNM4γ4 [26] (for which plaque size was reduced however) nor Φ12γ3 [27] (Fig. 1A). Similar results were obtained using a chromosomally expressed Ssc-CBASS (Fig. S1B). Consistent with previous reports [3], infection of liquid cultures with Φ80α-vir at different multiplicity of infection (MOI) showed that Ssc-CBASS confers robust immunity and enables a complete recovery of the bacterial population at low phage concentrations (Fig. 1B). In addition, enumeration of colony-forming units (CFU) immediately before and after phage infection at MOI 5 indicated that Φ80α-vir (Fig. 1C), but not the Ssc-CBASS-insensitive ΦNM4γ4 phage (Fig. S1C), causes loss of cell viability. This initial

reduction is followed by an increase in CFU (presumably due to the growth of uninfected cells) that reflects Ssc-CBASS-mediated immunity against Φ80α-vir. This was not observed after infection with ΦNM4γ4, where the CFU count decreased with time. As expected, plaque-forming units (PFU) enumerated in these samples were in line with the CFU counts, demonstrating the inability of Φ80α-vir to detectably propagate (Fig. 1D) compared to a steady increase in ΦNM4γ4 PFUs over time (Fig. S1D). Altogether these data show that, similarly to other species, CBASS defense protects staphylococcal populations by preventing the growth of infected hosts to limit viral propagation.

A 400-nucleotide phage RNA binds and activates Ssc-CdnE03

Next, we investigated how Ssc-CBASS is activated by Φ80α-vir. We first considered the possibility of transcriptional activation of the operon during infection, as was reported for the type III CBASS of *Escherichia coli* upec-117 [28]. RT-qPCR, however, failed to detect an increase in the transcription of the Ssc-CBASS genes upon infection (Fig. S2A). In addition, overexpression of the full operon, or either the cyclase or the effector alone, did not result in cell toxicity in the absence of phage (Fig. S2B). Therefore, we decided to look for CBASS activators by performing nucleotide synthesis assays *in vitro* using purified Ssc-CdnE03. We incubated the cyclase with trace ^{32}P-labeled NTPs and an excess of unlabeled NTPs and, following phosphatase treatment, we visualized the reaction products using thin-layer chromatography [9]. We tested *S. aureus* RN4220 crude lysate, purified Φ80α-vir particles, host genomic DNA, phage genomic DNA, and total RNA from both uninfected and infected *S. aureus* RN4220 cells. Strikingly, only RNA isolated from cells infected with Φ80α-vir enabled the generation of a cyclic

nucleotide product by wild-type Ssc-CdnE03 (Fig. 2A), but not the active site mutant D86A,D88A that fails to mediate immunity (Fig. S2C). To determine the cyclase product, we used different radiolabeled NTPs and found that ATP and GTP are both necessary and sufficient for product formation (Fig. S2D). Further analysis of this product by LC-MS defined it as an isomer (3',3' or 3',2') of cyclic guanosine monophosphate-adenosine monophosphate, cGAMP (Fig. S2E-F and Supplementary Text).

To identify the activating RNA species, we purified a hexahistidyl-tagged, maltose-binding protein fusion of Ssc-CdnE03, and immobilized it to a cobalt resin column that was loaded with total RNA extracted from either infected or uninfected staphylococci. Extraction and separation of the nucleic acids bound by the cyclase revealed the presence of an RNA that migrated at approximately 800 nucleotides in length (compared to an ssRNA ladder) that was pulled down only from the RNA fraction of infected, but not uninfected cells (Fig. 2B). We repeated this assay with RNA obtained from cells infected with other phages and isolated a similar species for the Ssc-CBASS-sensitive ΦNM1γ6 phage, but not for the resistant ΦNM4γ4 and Φ12γ3 viruses (Fig. 2C). We subjected both isolated RNA species to next-generation sequencing to determine their origin. For the Φ80α-vir RNA bound to the cyclase we found that reads mapped to a 400-nucleotide region beginning within the *gp40* gene and extending into *gp41*, which encode the terminase small and large subunits, TerS and TerL, respectively (Fig. 2D and Supplementary Sequences). Similar results were obtained for the cyclase-bound RNA generated during ΦNM1γ6 infection (Fig. S2G and Supplementary Sequences). We named this viral-derived RNA the "CBASS-activating bacteriophage RNA" (cabRNA). Interestingly, we also detected reads for a 400-

144 nucleotide host RNA derived from *addB*, which encodes one of the subunits of the
145 AddAB helicase/nuclease complex involved in homologous-directed DNA repair [29] (Fig.
146 S2H and Supplementary Sequences). This RNA was not detected in the material
147 pulled-down by the cyclase after incubation with total RNA from the host, in the absence
148 of phage infection, using RT-PCR. This result suggests that, as is the case for the
149 cabRNA, the host RNA associated with Ssc-CdnE03 is generated during the Φ80α-vir
150 lytic cycle. Finally, we purified the RNAs obtained during the pull-down assays and
151 found that they activate cGAMP production *in vitro* (Fig. S2I).

152 **Secondary structures within the cabRNA are required to activate Ssc-CdnE03**

153 The electrophoretic migration of the cabRNA, higher than its nucleotide length (runs
154 similarly to a ~800-nt ssRNA, but is actually 400-nt long), suggests the existence of
155 secondary structures that may be important for cyclase activation. Using ViennaRNA
156 software [30] to predict such structures, we found several hairpins and double-stranded
157 RNA (dsRNA) regions within the cabRNA (Fig. S3A). To test for the presence of these
158 structures in the species pulled down by the cyclase, we used RNases T1 and III, which
159 cleave ssRNA and dsRNA, respectively [31]. We found that RNase III completely
160 degraded the cabRNA, while RNase T1 did not affect this RNA (Fig. 3A). We also
161 treated the total RNA extracted from infected staphylococci with these RNases as well
162 as with another that degrades ssRNA, RNase A [31], and assayed for the ability of the
163 treated samples to induce cGAMP production by Ssc-CdnE03 (Fig. 3B). While both
164 RNases T1 and A degraded most of the RNA extracted from infected cells, the treated
165 samples were still able to activate the cyclase. In contrast, RNase III treatment showed
166 a limited impact on the degradation of the total RNA but completely abrogated the ability

of the total RNA to induce cGAMP production. These results demonstrate that dsRNAs, but not ssRNAs, produced during Φ80α-vir infection are important for Ssc-CdnE03 activation.

To determine if the cabRNA alone is sufficient for the activation of the cyclase, in the absence of other RNAs generated during infection, as well as to test the importance of RNA folding for this activation, we produced cabRNA *in vitro* using T7 RNA polymerase. The obtained transcript migrated similarly to a ssRNA of approximately 400 nucleotides after agarose gel electrophoresis and was completely digested by RNase T1 (Fig. 3C). This observation suggests that this *in vitro*-transcribed (IVT) cabRNA species lacks most of the secondary structures present in the cabRNA produced during infection. Therefore, we promoted the folding of the IVT cabRNA by heating it to 95°C for 5 minutes before slowly cooling the sample to room temperature. This treatment led to the generation of a cabRNA species with similar properties to that isolated from infected cells; i.e. migrated at ~ 800 nt and was resistant to RNase T1 degradation (Fig. 3C). We tested the ability of the unfolded and folded IVT cabRNA to activate the cyclase and found that whereas the folded species induced cGAMP synthesis to the same levels of the cabRNA produced *in vivo*, the unfolded species triggered the production of substantially lower quantities of the cyclic dinucleotide, which we attribute to a low level of spontaneous folding of the IVT cabRNA in the sample used for this assay (Fig. 3D). We also tested the activating properties of an IVT RNA with a sequence complementary to that of the cabRNA (transcribed using the same template DNA but in the opposite direction), as well as the 400-nucleotide host RNA (transcribed from *addB*) that was found bound to the cyclase and its complementary RNA, in all cases heated and cooled

to promote folding. None of these RNAs were found to activate Ssc-CdnE03 (Fig. S3A). Finally, we used synthetic RNA oligonucleotides with the sequences of the two most prominent predicted hairpins (hairpin-1 and -2, Fig. S3A) to determine their importance for cyclase activation. We found that, although at lower levels than the full cabRNA, hairpin-1, but not hairpin-2, induced cGAMP production (Fig. 3E). Other synthetic RNAs, including an unrelated hairpin structure, a dsRNA, and a ssRNA oligo (all with a similar size to hairpin-1 but with a different sequence, Table S5), failed to activate the cyclase. Altogether, these data indicate that specific secondary and/or tertiary structures within the cabRNA are essential for activation of Ssc-CdnE03.

We also investigated the ability of the cabRNA to activate Ssc-CBASS *in vivo*, in the absence of phage infection. To do this, we cloned the corresponding DNA sequence under the transcriptional control of an anhydrotetracycline (aTc)-inducible promoter on a staphylococcal expression vector [32]. Given the abortive infection mechanism detected after Φ80α-vir infection (Fig. 1B-D), we expected that, upon addition of aTc, induction of cGAMP synthesis by Ssc-CdnE03 and the subsequent activation of the membrane-disrupting effector would result in a proliferation defect and/or death of staphylococci. However, cabRNA transcription did not affect the growth of the cultures (Fig. S3C). To verify the plasmid-based expression of the cabRNA, we performed a pull-down assay using total RNA extracted from this strain after addition of aTc (Fig. S3D). Interestingly, most of the recovered cabRNA displayed an electrophoretic mobility consistent with the RNase T1-sensitive, unfolded form of the cyclase inducer (lower band). This observation suggests that the unfolded cabRNA can interact with, but not activate, Ssc-CdnE03. Given that mostly RNase III-sensitive, folded cabRNA is detected during pull-

down assays using total RNA extracted from infected cells (Figs. 2B-C and S3D), we speculate that Φ80α-vir infection is critical for the proper generation, modification, and/or folding of the inducer RNA.

A conserved, positively charged surface within Ssc-CdnE03 binds the cabRNA

To investigate how the cabRNA interacts with Ssc-CdnE03, we obtained a structure prediction using AlphaFold (Fig. 4A and S4A). Similar to other characterized CD-NTases, Ssc-CdnE03 shares structural features and organization with mammalian OAS1 and cGAS despite low sequence similarity (~20%) [33] (Fig. S4B). In particular, Ssc-CdnE03 and OAS1 share several core features: i) the common DNA polymerase β-like nucleotidyltransferase superfamily protein fold and conserved active site architecture, ii) a pocket on the backside of the active site with positive charge, iii) two positively charged residues (Arg and Lys) at the first helix of the PβCD domain, and iv) a surface exposed lysine and arginine along the enzyme "spine". (Fig. S4C). Importantly, these features are associated with the sensing of dsRNA for OAS1 [1,6,18]. To test if the positively charged surface of Ssc-CdnE03 is involved in cabRNA sensing, we substituted lysine residues present on this surface (K9, K13 Figs. 4A and S4C) for glutamic acid residues and assayed for cGAMP production *in vitro*. We found that the K9E and K13E substitutions substantially impaired the production of cGAMP in vitro and in vivo (Fig. 4B). To determine the role of this basic surface in cabRNA binding, we performed electrophoretic mobility shift assays using increasing concentrations of enzyme and observed that the substitution of K9, more than the K13E, notably affected the interaction of the cyclase with its inducer (Fig. 4C). Consistent with these *in vitro* results, CBASS immunity against Φ80α-vir was most severely abrogated by the K9E

mutation, and mildly reduced in staphylococci carrying the K13E mutant cyclase (Fig. 4D). Altogether these results demonstrate that the cabRNA interacts with a positively charged surface present in Ssc-CdnE03 to activate cGAMP synthesis and initiate the staphylococcal CBASS response.

Phage mutants that evade Ssc-CBASS immunity fail to produce cabRNA

To gain further insight into the mechanism of Ssc-CBASS induction, we sought to isolate phage mutants that can evade defense. Since we were unable to observe discrete Φ80α-vir or ΦNM1γ6 plaques in our assays (Fig. 1A), something previously observed for defense mechanisms that mediate abortive infection [34], we used ethyl methanesulfonate (EMS) to introduce random mutations into a Φ80α-vir population. Phages were plated on lawns of staphylococci harboring the Ssc-CBASS to isolate escape mutants that are able to form plaques (Fig. S5A). We then performed next-generation sequencing and detected Φ80α-vir escapers carrying mutations (Fig. S5B). Many of these phages harbored nucleotide substitutions within the *gp46* gene, which encodes the scaffold protein for the viral capsid [24]. This finding is consistent with recent reports of type II CBASS escape mutations in phage capsid genes [35,36]. Mutations generated missense amino acid substitutions in the scaffold protein and were corroborated to mediate the evasion of Ssc-CBASS immunity in infection and plaque formation assays; phenotypes that were reverted by the expression of wild-type Gp46 in the host (Fig. S5C-D). Next, we examined cabRNA production by these phages. Total RNA from staphylococci infected with phage expressing the *gp46*^{E105D} mutant or wild-type Φ80α-vir mediated similar levels of cGAMP synthesis *in vitro* (Fig. S5E). In addition, pull-down assays using immobilized Ssc-CdnE03 retrieved the same cabRNA

isolated from cells infected with wild-type viruses (Fig. 5D). Therefore, we conclude that these escapers that produce mutant capsids evade Ssc-CBASS immunity through a mechanism that does not affect the generation of cabRNA.

A different escaper mutation mapped to *terS*. This was a C to T transition that changes serine (UCU) 74 to phenylalanine (UUU) in this terminase subunit, located 6 nucleotides upstream of the cabRNA start. Infection of staphylococci harboring Ssc-CBASS with the Φ80α-vir(*terS*^{S74F}) mutant phage prevented bacterial growth (Fig. 5A), and resulted in the production of high numbers of viral particles (Fig. 5B). Total RNA from the infected cultures failed to stimulate cGAMP production (Fig. 5C). Surprisingly, pull-down assays revealed that the cyclase binds an RNA species generated during infection that is several hundreds of nucleotides larger than the cabRNA (Fig. 5D). RNA-seq of this species identified it as a 1,237-nt long transcript that starts at *gp39* [which encodes RinA, the transcriptional regulator of the late-expressed genes of Φ80α-vir [37]] and extends into *terL* (*gp41*), harbors the C to T mutation, and shares the same 3' end with the cabRNA (Fig. 2D and Supplementary Sequences). Interestingly, in contrast to the cabRNA, which is resistant to degradation by RNase T1 and completely susceptible to RNase III (Fig. 3A), the 1,237-nt escaper RNA isolated from the pull-down assay was susceptible to RNase T1 and was only partially degraded by RNase III (Fig. S6A). This RNA retained a low level of cyclase activation, which was eliminated after RNase III treatment (Fig. 5E). On the other hand, a synthetic escaper RNA generated through *in vitro* transcription failed to induce cGAMP production (Fig. S6B). Altogether these results indicate that the "long" escaper RNA has a different secondary/tertiary structure than the cabRNA. This long RNA species mediates low levels of Ssc-CdnE03 binding

and activation, but is not sufficient to trigger a full Ssc-CBASS response *in vivo*. Finally, we introduced the escape mutation into the *terS* homolog of ΦNM1γ6. We found that recombinant phages acquired resistance to Ssc-CBASS (Fig. S6C and Supplementary Sequences), a result that confirms that this *terS*^{S74F} mutation is sufficient to subvert Ssc-CBASS activation. Importantly, neither overexpression of wild-type TerS (Fig. S6D), Gp46 (Fig. S6E), nor the complete set of phage genes required for capsid formation (*gp40-gp47*, Fig. S6F), which expression was shown to form Φ80α capsids in the absence of phage infection [38], impaired the growth of staphylococci carrying the Ssc-CBASS system, indicating that TerS, Gp46 or the full Φ80α capsid, do not participate directly in Ssc-CdnE03 activation.

We also performed experiments to restore Ssc-CBASS immunity against Φ80α-vir(*terS*^{S74F}) through the overexpression of either wild-type TerS (from a plasmid, pTerS) or cabRNA. Protein expression during infection prevented both cell death (Fig. 5A) as well as mutant phage propagation (Fig. 5B) through the generation of a structured cabRNA (Fig. 5C-D). Since the pTerS construct introduced into staphylococci cannot produce the activating RNA (it lacks the *terL*-encoded, downstream half of the cabRNA), these data suggest that the terminase small subunit protein is required for the generation an activating cabRNA with the proper length. Infection of staphylococci expressing a plasmid-encoded cabRNA also reduced the propagation of Φ80α-vir(*terS*^{S74F}) (Fig. S6G). Interestingly, in contrast to the plasmid-expressed cabRNA isolated from uninfected cells, a greater fraction of the RNA pulled down by the cyclase from staphylococci overexpressing the plasmid-borne cabRNA and infected with Φ80α-vir(*terS*^{S74F}) displayed an electrophoretic mobility consistent with the structured form of

the cabRNA (Fig. S3D). This result supports our previous hypothesis that the secondary structures present in the inducer RNA, required for the activation of Ssc-CdnE03, are generated during phage infection.

DISCUSSION

Here we show that the cyclic dinucleotidyltransferase of the *S. schleiferi* type I-B CBASS binds a 400-nucleotide RNA transcribed from the staphylococcal phages Φ80α-vir and ΦNM1γ6 during infection, which we named cabRNA. This RNA forms secondary structures and interacts with a positively charged surface of the cyclase to promote the generation of cGAMP and initiate the CBASS anti-phage response. Most staphylococcal CBASS belong to the type I class and contain cyclases that are diverse phylogenetically, with many of them lacking the two positively charged residues at the first helix of the PβCD domain the surface exposed and conserved lysine or arginine residues along the spine and N-terminal domain that we identified as necessary for the interaction with the cabRNA (Fig. S7A). This suggests that there are other modes of cyclase activation, both in staphylococci and in other CBASS types, that do not sense viral RNA. This idea is also supported by our findings that the staphylococcal phages ΦNM4γ4 and Φ12γ3 do not produce cabRNA and are not restricted by Ssc-CBASS. Effective immunity against these phages may be provided by either the above-mentioned CBASS cyclases that sense viral signals different than the cabRNA, or by another, non-CBASS, mechanism of anti-phage defense. The positively charged surface made up of lysine and arginine residues in the N-terminal, PβCD, and C-terminal helices, however, are present in all members of the CdnE03 family of cyclases

(Fig. S7B). These are widely distributed in different organisms and therefore we believe that the recognition of viral RNA for the activation of CBASS is a widespread mechanism across prokaryotes. Interestingly, the size of this surface (approximately 40 Å in length) should be able to only accommodate a dsRNA of approximately 20 base pairs, and therefore it remains incompletely understood which region of the cabRNA is most important for cyclase activation. We tested the two sequences with the strongest probability of hairpin formation within the cabRNA and found that only one mediated substantial, but not complete, activation (Fig. 3E). Therefore, it is possible that multiple Ssc-CdnE03 enzymes bind to the cabRNA to achieve high levels of cGAMP synthesis. This mechanism of activation is similar to that of human OAS1 and OAS3, which also require large dsRNA molecules for optimal activity [39]. In the case of OAS1, the positively charged surface can interact with approximately with 18-20 base pairs (Fig. S4B). However, dsRNAs of this length can only provide limited activity (~7-8% of the maximum) [39], therefore it is likely that longer species are also being recognized by OAS1 during viral infection *in vivo*. In OAS1, dsRNA binding leads to the rearrangement of the N and C lobes of the enzyme that positions the active site residues in the appropriate conformation for catalysis [33]. Eukaryotic cyclases are activated by long, unmodified dsRNA in a sequence-independent manner, since since the presence of these molecules in the cytoplasm usually signals infection by RNA viruses [15]. Given the lack of nuclear compartmentalization in bacteria, our results suggest that prokaryotic CBASS cyclases require a specific phage-derived structured RNA to avoid the autoimmunity that would be induced by host-derived transcripts.

It is not currently known how the cabRNA is produced during infection. Given that expression of a cabRNA in uninfected hosts results generates mostly the unfolded version of this species (Fig. S3D), which is pulled down by the Ssc-CdnE03 cyclase but fails to activate the CBASS response (Fig. S3C), we speculate that phage infection is required for the folding of the cabRNA into its cyclase-activating form. In addition, the S74F mutation in TerS, which does not change the cabRNA sequence, leads to the production of a longer, non-activating form of the cabRNA (Fig. 5D). This size change can be rescued *in trans* by the expression of wild-type TerS (Fig. 5D) and therefore we conclude that this protein is required to determine the proper length of the cabRNA. Interestingly, we and others [35,36] found mutations in capsid proteins (Gp46 in the case of Φ80α-vir) that enable escape from CBASS immunity. A structured cabRNA is produced during infection by these mutants (Fig. 5D) that is capable of fully activating the Ssc-CdnE03 cyclase (Fig S5E). In addition, compared to the *terS*^{S74F} mutant phages, the *gp46*^{E105D} escapers completely kill staphylococci in liquid cultures (Fig. S5C, compare to Fig. 5A) and form larger plaques in agar plates (Fig. S5A, compared to Fig. 5B). Therefore, we hypothesize that capsid mutations interfere with Ssc-CBASS immunity after cGAMP production. Finally, our pull-down assays also detected a host-derived RNA of the same length as the cabRNA. This RNA was not pulled down by Ssc-CdnE03 from total RNA of uninfected cells [nucleic acids were not detected after elution and agarose gel electrophoresis (Fig. 2B), nor by RT-PCR of the eluate (data not shown)]. Since it is not required for activation of cGAMP production *in vitro*, we speculate that the host RNA could perhaps be pulled down due to base-pair interactions with the cabRNA. However, given that these RNAs have identical lengths, we cannot

rule out the possibility that the host RNA also has a function in Ssc-CBASS immunity *in vivo*. Future studies will elucidate the details of the biogenesis of the cabRNA and host-derived RNA during infection, as well as their molecular interactions with CdnE03 enzymes to initiate the synthesis of cyclic nucleotide second messengers.

REFERENCES

1 Burroughs, A. M., Zhang, D., Schaffer, D. E., Iyer, L. M. & Aravind, L. Comparative genomic analyses reveal a vast, novel network of nucleotide-centric systems in biological conflicts, immunity and signaling. *Nucleic Acids Res.* **43**, 10633-10654, (2015).

2 Wein, T. & Sorek, R. Bacterial origins of human cell-autonomous innate immune mechanisms. *Nat. Rev. Immunol.* **22**, 629-638, (2022).

3 Cohen, D. *et al.* Cyclic GMP-AMP signalling protects bacteria against viral infection. *Nature* **574**, 691-695, (2019).

4 Millman, A., Melamed, S., Amitai, G. & Sorek, R. Diversity and classification of cyclic-oligonucleotide-based anti-phage signalling systems. *Nat Microbiol* **5**, 1608-1615, (2020).

5 Burdette, D. L. *et al.* STING is a direct innate immune sensor of cyclic di-GMP. *Nature* **478**, 515-518, (2011).

6 Sun, L., Wu, J., Du, F., Chen, X. & Chen, Z. J. Cyclic GMP-AMP synthase is a cytosolic DNA sensor that activates the type I interferon pathway. *Science* **339**, 786-791, (2013).

7 Davies, B. W., Bogard, R. W., Young, T. S. & Mekalanos, J. J. Coordinated regulation of accessory genetic elements produces cyclic di-nucleotides for V. cholerae virulence. *Cell* **149**, 358-370, (2012).

8 Krasteva, P. V. & Sondermann, H. Versatile modes of cellular regulation via cyclic dinucleotides. *Nat. Chem. Biol.* **13**, 350-359, (2017).

9 Whiteley, A. T. *et al.* Bacterial cGAS-like enzymes synthesize diverse nucleotide signals. *Nature* **567**, 194-199, (2019).

10 Ye, Q. *et al.* HORMA Domain Proteins and a Trip13-like ATPase Regulate Bacterial cGAS-like Enzymes to Mediate Bacteriophage Immunity. *Mol. Cell* **77**, 709-722 e707, (2020).

11 Ablasser, A. *et al.* cGAS produces a 2'-5'-linked cyclic dinucleotide second messenger that activates STING. *Nature* **498**, 380-384, (2013).

12 Gao, P. *et al.* Cyclic [G(2',5')pA(3',5')p] is the metazoan second messenger produced by DNA-activated cyclic GMP-AMP synthase. *Cell* **153**, 1094-1107, (2013).

13 Diner, E. J. *et al.* The innate immune DNA sensor cGAS produces a noncanonical cyclic dinucleotide that activates human STING. *Cell Rep* **3**, 1355-1361, (2013).

14 Zhang, X. *et al.* Cyclic GMP-AMP containing mixed phosphodiester linkages is an endogenous high-affinity ligand for STING. *Mol. Cell* **51**, 226-235, (2013).

15 Wu, J. & Chen, Z. J. Innate immune sensing and signaling of cytosolic nucleic acids. *Annu. Rev. Immunol.* **32**, 461-488, (2014).

16 de Oliveira Mann, C. C., Kiefersauer, R., Witte, G. & Hopfner, K. P. Structural and biochemical characterization of the cell fate determining nucleotidyltransferase fold protein MAB21L1. *Sci Rep* **6**, 27498, (2016).

17 Slavik, K. M. *et al.* cGAS-like receptors sense RNA and control 3'2'-cGAMP signalling in Drosophila. *Nature* **597**, 109-113, (2021).

18 Schwartz, S. L. *et al.* Human OAS1 activation is highly dependent on both RNA sequence and context of activating RNA motifs. *Nucleic Acids Res.* **48**, 7520-7531, (2020).
19 Zhu, D. *et al.* Structural biochemistry of a Vibrio cholerae dinucleotide cyclase reveals cyclase activity regulation by folates. *Mol. Cell* **55**, 931-937, (2014).
20 Misic, A. M., Cain, C. L., Morris, D. O., Rankin, S. C. & Beiting, D. P. Complete Genome Sequence and Methylome of Staphylococcus schleiferi, an Important Cause of Skin and Ear Infections in Veterinary Medicine. *Genome Announc* **3**, (2015).
21 Duncan-Lowey, B., McNamara-Bordewick, N. K., Tal, N., Sorek, R. & Kranzusch, P. J. Effector-mediated membrane disruption controls cell death in CBASS antiphage defense. *Mol. Cell* **81**, 5039-5051 e5035, (2021).
22 Horinouchi, S. & Weisblum, B. Nucleotide sequence and functional map of pC194, a plasmid that specifies inducible chloramphenicol resistance. *J. Bacteriol.* **150**, 815-825, (1982).
23 Kreiswirth, B. N. *et al.* The toxic shock syndrome exotoxin structural gene is not detectably transmitted by a prophage. *Nature* **305**, 709-712, (1983).
24 Christie, G. E. *et al.* The complete genomes of Staphylococcus aureus bacteriophages 80 and 80alpha--implications for the specificity of SaPI mobilization. *Virology* **407**, 381-390, (2010).
25 Goldberg, G. W., Jiang, W., Bikard, D. & Marraffini, L. A. Conditional tolerance of temperate phages via transcription-dependent CRISPR-Cas targeting. *Nature* **514**, 633-637, (2014).
26 Heler, R. *et al.* Cas9 specifies functional viral targets during CRISPR-Cas adaptation. *Nature* **519**, 199-202, (2015).
27 Modell, J. W., Jiang, W. & Marraffini, L. A. CRISPR-Cas systems exploit viral DNA injection to establish and maintain adaptive immunity. *Nature* **544**, 101-104, (2017).
28 Blankenchip, C. L. *et al.* Control of bacterial immune signaling by a WYL domain transcription factor. *Nucleic Acids Res.* **50**, 5239-5250, (2022).
29 Wigley, D. B. Bacterial DNA repair: recent insights into the mechanism of RecBCD, AddAB and AdnAB. *Nat. Rev. Microbiol.* **11**, 9-13, (2013).
30 Lorenz, R. *et al.* ViennaRNA Package 2.0. *Algorithms Mol Biol* **6**, 26, (2011).
31 Bechhofer, D. H. & Deutscher, M. P. Bacterial ribonucleases and their roles in RNA metabolism. *Crit. Rev. Biochem. Mol. Biol.* **54**, 242-300, (2019).
32 Rostol, J. T. & Marraffini, L. A. Non-specific degradation of transcripts promotes plasmid clearance during type III-A CRISPR-Cas immunity. *Nat Microbiol* **4**, 656-662, (2019).
33 Donovan, J., Dufner, M. & Korennykh, A. Structural basis for cytosolic double-stranded RNA surveillance by human oligoadenylate synthetase 1. *Proc Natl Acad Sci U S A* **110**, 1652-1657, (2013).
34 Meeske, A. J., Nakandakari-Higa, S. & Marraffini, L. A. Cas13-induced cellular dormancy prevents the rise of CRISPR-resistant bacteriophage. *Nature* **570**, 241-245, (2019).
35 Huiting, E. *et al.* Bacteriophages antagonize cGAS-like immunity in bacteria. *bioRxiv*, 2022.2003.2030.486325, (2022).

36 Stokar-Avihail, A. *et al.* Discovery of phage determinants that confer sensitivity to bacterial immune systems. *bioRxiv*, 2022.2008.2027.505566, (2022).
37 Ferrer, M. D. *et al.* RinA controls phage-mediated packaging and transfer of virulence genes in Gram-positive bacteria. *Nucleic Acids Res.* **39**, 5866-5878, (2011).
38 Spilman, M. S. *et al.* Assembly of bacteriophage 80alpha capsids in a Staphylococcus aureus expression system. *Virology* **434**, 242-250, (2012).
39 Wang, Y., Holleufer, A., Gad, H. H. & Hartmann, R. Length dependent activation of OAS proteins by dsRNA. *Cytokine* **126**, 154867, (2020).
40 Horinouchi, S. & Weisblum, B. Nucleotide sequence and functional map of pE194, a plasmid that specifies inducible resistance to macrolide, lincosamide, and streptogramin type B antibodies. *J. Bacteriol.* **150**, 804-814, (1982).
41 Jakociune, D. & Moodley, A. A Rapid Bacteriophage DNA Extraction Method. *Methods Protoc* **1**, (2018).
42 Maguin, P., Varble, A., Modell, J. W. & Marraffini, L. A. Cleavage of viral DNA by restriction endonucleases stimulates the type II CRISPR-Cas immune response. *Mol. Cell* **82**, 907-919 e907, (2022).
43 Galaxy, C. The Galaxy platform for accessible, reproducible and collaborative biomedical analyses: 2022 update. *Nucleic Acids Res.* **50**, W345-351, (2022).

Acknowledgements. We would like to thank the members of the Marraffini laboratory for constructive feedback and encouragement, and Shelley Rankin at the University of Pennsylvania School of Veterinary Medicine for isolates of *S. schleiferi* 2142-05, 2317-03, and 5909-02. DVB is supported by an NIH Ruth L. Kirschstein NRSA F30 Individual Predoctoral Fellowship (F30AI157535) and an NIH Medical Scientist Training Program grant (T32GM007739) to the Weill Cornell/Rockefeller/Sloan Kettering Tri-Institutional MD-PhD Program. Support for this work comes from the National Institute of Health Director's Pioneer Award 1DP1GM128184-01 to LAM. LAM is an investigator of the Howard Hughes Medical Institute.

Authors contributions. Experiments were designed and analyzed by DVB, CR and LAM. CR and DVB conducted all experiments, except LC/MS of Ssc-CdnE03 products, which was performed by AMA. The paper was written by CR, DVB and LAM with the help and approval of all the authors.

Competing interests: L.A.M. is a cofounder and Scientific Advisory Board member of Intellia Therapeutics, and a co-founder of Eligo Biosciences.

Data and materials availability: all the data from these studies are available from the authors upon request.

Supplementary Materials

Materials and Methods
Supplementary Text
Tables S1 – S5
Supplementary Sequences
Figs. S1 – S7

FIGURE LEGENDS

Figure 1. CBASS confers anti-bacteriophage defense in staphylococci via abortive infection (A) Detection of phage propagation after spotting ten-fold dilutions of the lytic DNA phages, Φ80α-vir, ΦNM1γ6, ΦNM4γ4, and Φ12γ3 onto lawns of *S. aureus* RN4220 harboring a plasmid-borne either incomplete (Ssc-CdnE03 alone) or intact Ssc-CBASS operon. **(B)** Growth of staphylococci harboring either an incomplete (Ssc-CdnE03 alone) or intact Ssc-CBASS operon measured by optical density at 600 nm after the addition of Φ80α-vir at a multiplicity of infection (MOI) of 0, 0.1, 1, or 10. The mean of three biological replicates ± SD is reported. **(C)** Enumeration of colony-forming units (CFU) from cultures harboring Ssc-CdnE03 alone or Ssc-CBASS immediately before infection (Pre), after initial absorption of the phage (0 h), after one lytic cycle (1 h), and after complete culture lysis (3 h) by Φ80α-vir at MOI 5. Mean ± SEM of three biological replicates is reported. **(D)** Same as **(C)** but enumerating of plaque-forming units (PFU). Mean ± SEM of three biological replicates is reported.

Figure 2. A viral RNA produced during infection activates Ssc-CdnE03 *in vitro* (A) Thin-layer chromatography analysis of Ssc-CdnE03 products in the presence of the following: *S. aureus* RN4220 crude lysate, whole purified Φ80α-vir particles, host genomic DNA (RN4220 gDNA), phage gDNA, and total RNA from *S. aureus* RN4220 in the presence or absence of Φ80α-vir infection (before the completion of 1 lytic cycle). A representative image of multiple replicates is shown. An agarose gel stained with ethidium bromide (middle) and SDS-PAGE stained with Coomassie blue (bottom) are shown as loading controls. Pi, free phosphates; int, intermediate cyclase product; cdn,

cyclic dinucleotide. **(B)** Agarose gel electrophoresis of the input and output RNA obtained after incubation of Ssc-CdnE03 with no RNA, total RNA extracted from uninfected staphylococci (RN4220) or from cells infected with Φ80α-vir phage. An SDS-PAGE stained with Coomassie blue (bottom) is shown as a loading control. **(C)** Same as in **(B)**, but with input RNA extracted from staphylococci infected with ΦNM1γ6, Φ80α-vir, ΦNM4γ4, or Φ12γ3 phages. **(D)** Diagram of ϕ80α-vir and ϕ80α-vir(*terS*^{S74F}) genomes with localization of the cabRNA and escaper RNA sequences, respectively. The location of the escaper mutation, C221>T, is shown.

Figure 3. Secondary structures within the cabRNA are required for Ssc-CdnE03 activation. (A) Agarose gel electrophoresis of pulled-down cabRNA treated with RNases T1 or III. **(B)** Thin-layer chromatography analysis of Ssc-CdnE03 products in the presence of total RNA extracted from infected cells and treated with RNases III, A, T1, or untreated. A representative image of multiple replicates is shown. An agarose gel stained with ethidium bromide (middle) and SDS-PAGE stained with Coomassie blue (bottom) are shown as loading controls. Pi, free phosphates; int, intermediate cyclase product. **(C)** Agarose gel electrophoresis of *in vitro* transcribed (IVT) cabRNA, unfolded (left) and folded (right), untreated or treated with RNase T1. **(D)** Same as in **(B)** but incubating the cyclase with pulled-down, unfolded or folded IVT cabRNA. **(E)** Same as in **(B)** but incubating the cyclase with pulled-down RNA or different synthetic RNA oligonucleotides.

554 **Figure 4. A positively charged surface within Ssc-CdnE03 binds the cabRNA to**
555 **initiate immunity. (A)** AlphaFold model of Ssc-CdnE03 displayed with surface
556 electrostatics (-77 to 77, red to blue). Inset, positively charged region harboring the
557 mutated lysine residues 9 and 13. **(B)** Thin-layer chromatography analysis of the
558 products of different Ssc-CdnE03 mutants in the presence of total RNA extracted from
559 infected cells. A representative image of multiple replicates is shown. An agarose gel
560 stained with ethidium bromide (middle) and SDS-PAGE stained with Coomassie blue
561 (bottom) are shown as loading controls. Pi, free phosphates; int, intermediate cyclase
562 product. **(C)** Electrophoretic mobility shift assay of cabRNA in the presence of
563 increasing concentrations of different Ssc-CdnE03 mutants. **(D)** Growth of staphylococci
564 harboring the Ssc-CBASS operon with wild-type, K9E or K13E, Ssc-CdnE03 measured
565 by optical density at 600 nm after infection with Φ80α-vir at an MOI of 10. The mean of
566 three biological replicates ± SD is reported.
567
568 **Figure 5. Phage mutants that evade Ssc-CBASS immunity fail to produce**
569 **cabRNA. (A)** Growth of staphylococci harboring either an incomplete (Ssc-CdnE03
570 alone) or intact Ssc-CBASS operon measured by optical density at 600 nm after
571 infection with ϕ80α-vir or ϕ80α-vir(*terS*^{S74F}) at MOI 1, the latter in the presence or
572 absence of TerS overexpression using plasmid pTerS. The mean of three biological
573 replicates ± SD is reported. **(B)** Detection of phage propagation after spotting ten-fold
574 dilutions of Φ80α-vir or ϕ80α-vir(*terS*^{S74F}) onto lawns of *S. aureus* RN4220 harboring
575 either an incomplete (Ssc-CdnE03 alone) or intact Ssc-CBASS operon, the latter in the
576 presence or absence of TerS overexpression using plasmid pTerS. **(C)** Thin-layer

chromatography analysis of Ssc-CdnE03 products the presence of total RNA extracted from either uninfected staphylococci or cells infected with Φ80α-vir or Φ80α-vir(*terS*^{S74F}), the latter in the presence or absence of TerS overexpression using plasmid pTerS. A representative image of multiple replicates is shown. An agarose gel stained with ethidium bromide (middle) and SDS-PAGE stained with Coomassie blue (bottom) are shown as loading controls. Pi, free phosphates; int, intermediate cyclase product. **(D)** Agarose gel electrophoresis of the input and output RNA obtained after incubation of Ssc-CdnE03 with total RNA extracted from uninfected staphylococci (RN4220) or from cells infected with Φ80α-vir, Φ80α-vir(*gp46*^{E105D}) or Φ80α-vir(*terS*^{S74F}), the latter in the presence or absence of TerS overexpression using plasmid pTerS. **(E)** Same as **(C)** but in the presence of cabRNA, escaper RNA, or escaper RNA pre-treated with RNase III.

Figure S1. Type I-B CBASS immunity in staphylococci. (A) Schematic of the type I-B CBASS operon present in *Staphylococcus schleiferi* (*Ssc*) 2142-05, 2317-03, and 5909-02 genomes, flanked by a type I restriction-modification system. The CBASS operon consists of two genes encoding a cyclase belonging to the E clade, cluster 3 (Ssc-CdnE03) and a two-transmembrane domain-containing effector, Cap15. **(B)** Detection of phage propagation after spotting ten-fold dilutions of the lytic DNA phages, Φ80α-vir, ΦNM1γ6, ΦNM4γ4, and Φ12γ3 onto lawns of *S. aureus* RN4220 harboring either an incomplete (Ssc-CdnE03 alone) or intact Ssc-CBASS operon integrated in its genome. **(C)** Enumeration of colony-forming units (CFU) from cultures harboring Ssc-CdnE03 alone or Ssc-CBASS immediately before infection (Pre), after initial absorption

of the phage (0 h), after one lytic cycle (1 h), and after complete culture lysis (3 h) by ΦNM4γ4 at MOI 5. Mean ± SEM of three biological replicates is reported. **(D)** Same as **(C)** but enumerating of plaque-forming units (PFU). Mean ± SEM of three biological replicates is reported.

Figure S2. Regulation of Ssc-CBASS operon. (A) Expression of the Ssc-CdnE03 and Ssc-Cap15 effector genes during log-phase growth of *S. aureus* RN4220::Ssc-CBASS in the presence or absence of infection by Φ80α-vir measured by RT-qPCR. For each condition, expression ratios were determined by normalizing Cq values for Ssc-CBASS genes to Cq values for the housekeeping gene *glcC*. The mean of three biological replicates ± SEM is reported. **(B)** Growth of staphylococci harboring an over-expression plasmid containing either the Ssc-CdnE03 alone, Ssc-Cap15 alone, or the intact Ssc-CBASS operon under the transcriptional control of a P-spac promoter, measured by optical density at 600 nm after the addition of IPTG. The mean of three biological replicates ± SD is reported. **(C)** Growth of staphylococci harboring either an incomplete (Ssc-CdnE03 alone) or intact Ssc-CBASS operon, with either wild-type or D86A,D88A mutant Ssc-CdnE03, measured by optical density at 600 nm after the addition of Φ80α-vir at a MOI of 1. The mean of three biological replicates ± SD is reported. **(D)** Thin-layer chromatography analysis of Ssc-CdnE03 products in the presence of total RNA from *S. aureus* RN4220 after Φ80α-vir infection, using different radiolableled nucleotides to investigate the nucleotide composition of the enzymatic product. Pi, free phosphates; int, intermediate cyclase product; cdn, cyclic dinucleotide. **(E)** TIC of the reaction products of wild-type Ssc-CdnE03. The peak at retention time 4.36 minutes

coincides with the retention time of the isomers 3´,2´-cGAMP and 3´,3´-cGAMP. This peak is not present in the reaction products of the active site mutant cyclase, D86A-D88A. **(F)** Comparison of averaged MS/MS spectra of the reaction products of wild-type Ssc-CdnE03 (purple spectrum) and 3´,2´-cGAMP and 3´,3´-cGAMP (green spectrum). The most abundant ions are present in both samples (see Supplementary Text for a complete MS analysis). **(G)** Diagram of the ϕ80α-vir genome showing the localization of the cabRNA sequence. **(H)** Diagram showing the localization of the host RNA and escaper host RNA in the *addAB* operon of *S. aureus* RN4220. **(I)** Thin-layer chromatography analysis of Ssc-CdnE03 reaction products in the presence of cabRNA isolated from a pulldown assay. An agarose gel stained with ethidium bromide (middle) and SDS-PAGE stained with Coomassie blue (bottom) are shown as loading controls. Pi, free phosphates; int, intermediate cyclase product.

Figure S3. Analysis of cabRNA activation of Ssc-CdnE03. (A) Predicted structure of activating RNA. Secondary structure was predicted using ViennaRNA software. Model confidence for each nucleotide is shown as different colors: >=90% (red), 70-89% (orange), 50-60% (light blue), <50% (dark blue). **(B)** Thin-layer chromatography analysis of Ssc-CdnE03 reaction products in the presence of the cabRNA isolated from a pulldown assay, or the sense or antisense strands of *in vitro* transcribed (IVT) cabRNA and host RNA. All IVT RNA was subjected to heat refolding (see Methods). An agarose gel stained with ethidium bromide (middle) and SDS-PAGE stained with Coomassie blue (bottom) are shown as loading controls. Pi, free phosphates; int, intermediate cyclase product. **(C)** Growth of staphylococci harboring either an incomplete (Ssc-

CdnE03 alone, "-") or intact Ssc-CBASS ("+") operon and an empty vector ("-") or a plasmid encoding cabRNA ("+") under the control of an ATc inducible promoter measured by optical density at 600 nm. The mean of three biological replicates ± SD is reported. **(D)** Agarose gel electrophoresis of the input and output RNA obtained after incubation of Ssc-CdnE03 with total RNA extracted from cells infected with Φ80α-vir or Φ80α-vir(*terS*^{S74F}) phage, in the presence or absence of cabRNA plasmid overexpression.

Figure S4. Structural analysis of Ssc-CdnE03. (A) AlphaFold rank #1 model of Ssc-CdnE03 (top) with surface electrostatics shown (bottom). Black lines define a conserved primary dsRNA-binding surface present in porcine OAS1. **(B)** Crystal structure of porcine OAS1 bound to dsRNA (PDB: 4RWO) (top) with surface electrostatics shown (bottom). Black lines define the dsRNA-binding surface. **(C)** Structural alignment of Ssc-CdnE03 (red) and crystal structure of porcine OAS1:dsRNA (PDB: 4RWO) (blue) with zoomed-in cutaways highlighting conservation of the active site (top inset) and positively charged residues within the ligand binding surface (bottom inset).

Figure S5. Isolation and characterization of CBASS escapers. (A) An overnight culture of *S. aureus* RN4220 was diluted and outgrown to early log-phase, at which time Φ80α-vir at an MOI of 1 was added. Just before the first burst (~30 min), 1% ethyl methanesulfonate (EMS) was added to generate mutations. Infections in the presence of EMS were allowed to proceed at 37°C for 4 hours to allow phage to propagate and lyse the culture. Culture supernatants were collected, serially diluted, and spotted on a

669 lawn of *S. aureus* RN4220::Ssc-CBASS or Ssc-CdnE03. A control experiment without
670 the addition of the EMS mutagen is shown as control. **(B)** Diagram of ϕ80α-vir genome
671 with localization of four unique escaper mutations identified in *terS* or *gp46*. **(C)** Growth
672 of staphylococci harboring either an incomplete (Ssc-CdnE03 alone) or intact Ssc-
673 CBASS operon measured by optical density at 600 nm after the addition of Φ80α-vir or
674 ϕ80α-vir(*gp46*^{E105D}) at MOI 1. The mean of three biological replicates ± SD is reported.
675 **(D)** Detection of phage propagation after spotting ten-fold dilutions of Φ80α-vir or ϕ80α-
676 vir(*gp46*^{E105D}) onto lawns of *S. aureus* RN4220 harboring either an incomplete (Ssc-
677 CdnE03 alone) or intact Ssc-CBASS operon, the latter in the presence or absence of
678 Gp46 overexpression using plasmid pGp46. **(E)** Thin-layer chromatography analysis of
679 Ssc-CdnE03 reaction products in the presence of total RNA extracted from uninfected
680 staphylococci or cells infected with wild-type or *gp46*^{E105D} Φ80α-vir. Agarose gel
681 electrophoresis of RNA samples is displayed as a loading control.
682
683 **Figure S6. Mechanism of escape mediated by the *terS* mutation. (A)** Agarose gel
684 electrophoresis of the escaper RNA generated during infection with ϕ80α-vir(*terS*^{S74F})
685 isolated from a pulldown assay, treated with RNase T1 or III. **(B)** Thin-layer
686 chromatography analysis of Ssc-CdnE03 reaction products in the presence of cabRNA
687 or *in vitro* transcribed escaper RNA. **(C)** Wild-type ΦNM1γ6 was propagated in liquid
688 cultures of *S. aureus* RN4220::Ssc-CBASS harboring a plasmid-borne *terS* gene, wild-
689 type or S74F. Culture supernatants were collected and serial dilutions were spotted
690 onto lawns of *S. aureus* RN4220::Ssc-CdnE03 or RN4220::Ssc-CBASS. **(D)** Growth of
691 staphylococci harboring pTerS, providing IPTG-inducible expression of the Φ80α-vir

692 TerS protein, measured by optical density at 600 nm after the addition of the inducer.
693 The mean of three biological replicates ± SD is reported. **(E)** Same as **(D)** but using
694 pGp46 plasmid, providing IPTG-inducible expression of the Φ80α-vir Gp46 protein. **(F)**
695 Same as **(D)** but using pGp40-47 plasmid, providing IPTG-inducible expression of the
696 complete Φ80α-vir viral capsid. **(G)** Enumeration of plaque-forming units (PFU) from
697 cultures harboring Ssc-CdnE03 alone ("-") or Ssc-CBASS ("+") and either an empty
698 vector ("-") or a plasmid with cabRNA ("+") under the control of an aTc-inducible
699 promoter.
700
701 **Figure S7. Sequence analysis of CdnE03s (A)** Alignment of porcine OAS1, *D. erecta*
702 cGLR, and bacterial CdnE03s and **(B)** Alignment of CD-NTases from staphylococcal
703 species. The EhD[X_{50-90}]D catalytic triad is highlighted with a red outline and the
704 residues that make up the ligand binding site are highlighted with a blue outline.
705 Predicted basic ligand binding residues selected for mutational analysis are denoted
706 with black stars (*= conserved in bacteria, **= conserved in bacteria and OAS1).

MATERIALS AND METHODS:

Bacterial strains and growth conditions: The bacterial strains used in this study are listed in Supplementary Table S1. *Staphylococcus aureus* strain RN4220 [23] was grown at 37°C with shaking (220 RPM) in brain heart infusion (BHI) broth, supplemented with chloramphenicol (10 μg mL^{-1}) or erythromycin (10 μg mL^{-1}) to maintain pC194-based [22] or pE194-based plasmids [40], respectively. Cultures were supplemented with chloramphenicol (5 μg mL^{-1}) to select for strains with chromosomally integrated Ssc-CBASS or Ssc-CdnE03. Gene expression was induced by the addition of 1 mM isopropyl-d-1-thiogalactopyranoside (IPTG) or 100 ng mL^{-1} anhydrotetracycline (aTc), where appropriate.

Bacteriophage propagation: The bacteriophages used in this study are listed in Supplementary Table S2. To generate a high-titer phage stock, an overnight culture of *S. aureus* RN4220 was diluted 1:100 and outgrown to mid-log phase (~90 min) in BHI broth supplemented with 5 mM $CaCl_2$. The culture was diluted to an optical density measurement at 600 nm (OD_{600}) of 0.5 (~$1x10^8$ CFU mL^{-1}). The culture was infected by adding phage at a multiplicity of infection (MOI) of 0.1 (~$1x10^7$ PFU mL^{-1}), or by inoculating with either a single picked plaque or scrape of a frozen stock. The infected culture was grown at 37°C with shaking and monitored for lysis (full loss of turbidity was typically observed ~3-4 hr). Culture lysates were centrifugated (4,300 x g for 10 min) to pellet cellular debris. The supernatant was collected, passed through a sterile membrane filter (0.45 μm), and stored at 4°C. Phage concentrations were determined by serially diluting the obtained stock in 10-fold increments and spotting 5 μL of each dilution on BHI soft agar mixed with RN4220 and supplemented with 5 mM $CaCl_2$. After incubation overnight at 37°C, individual plaques (i.e. zones of no bacterial growth) were counted, and the viral titer was calculated.

Molecular cloning: The plasmids (and details of their construction) and the oligonucleotide primers used in this study are listed in Supplementary Tables S3 and S4, respectively. The coding sequences of Ssc-CBASS and phage gene products were obtained from genomic DNA preparations of *S. schleiferi* 2145-05 cultures [20] or phage stocks [41], respectively.

Chromosomal integration of Ssc-CBASS: Ssc-CBASS or Ssc-CdnE03, along with a chloramphenicol resistance (cmR) cassette, was integrated into the *hsdR* gene (which encodes the defective R-subunit of the restriction-modification system in *S. aureus* RN4220), an insertion site which was previously shown to not impact growth [42]. Ssc-CBASS-cmR and Ssc-CdnE03-cmR were amplified from the plasmids pDVB303 and pDVB301 respectively, using primers oDVB565 and oDVB566, which were flanked with loxP sites at both ends followed by 60-bp homology regions to *hsdR*. Electrocompetent *S. aureus* RN4220 cells harboring the recombineering plasmid pPM300 were electroporated with 1-2 μg of PCR product and selected for with chloramphenicol (5 μg mL^{-1}). Potential integrants were screened by colony PCR as well as for functional immunity, and then verified by Sanger sequencing.

Isolation of strictly lytic phage mutants: To construct a virulent mutant of the phage Φ80α [24], we used a variation of a method previously described to generate ΦNM1γ6 [25], ΦNM4γ4 [26], and Φ12γ3 [27]. Φ80α-vir was isolated as a spontaneous escaper forming a

clear plaque following Φ80α infection of a BHI soft agar lawn of *S. aureus* RN4220 cells harboring plasmid pDVB08, which encodes a type III-A CRISPR-Cas system targeting the Φ80α cI-like repressor. PCR of the Φ80α-vir *cI* gene and Sanger sequencing confirmed an 8-bp deletion.

Soft agar phage infection: 100 μL of an overnight bacterial culture was mixed with 5 mL BHI soft agar supplemented with 5 mM $CaCl_2$ and poured onto BHI agar plates to solidify at room temperature (~15 min). Phage lysates were serially diluted 10-fold and 4 μL was spotted onto the soft agar surface. Once dry, plates were incubated at 37°C overnight and visualized the next day. Individual plaques (zones of no bacterial growth) were enumerated manually.

Liquid culture phage infection: Overnight cultures were diluted 1:100 in BHI supplemented with 5 mM $CaCl_2$ and the appropriate antibiotic for selection, outgrown at 37°C with shaking to mid-log phase (~90 min), and normalized to OD_{600} 0.5. For the desired MOI, a calculated volume of phage stock was added to each culture and 150 μL was seeded into each well of a 96-well plate. OD_{600} was measured every 10 min in a microplate reader (TECAN Infinite 200 PRO) at 37°C with shaking.

RT-qPCR: Total RNA was extracted from *S. aureus* cells using a Direct-Zol™ RNA MiniPrep Plus Kit (Cat. R2072). Extracted RNA was treated with TURBO™ DNase (Thermo Fisher Scientific) before cDNA first-strand synthesis with SuperScript IV Reverse Transcriptase (Thermo Fisher Scientific) using random hexamers. qPCR was performed using Fast SYBR Green Master Mix (Life Technologies) and 7900HT Fast Real-Time PCR System (Applied Biosystems) with primer pairs for the *S. aureus* housekeeping gene *ptsG* (oDVB426/427), Ssc-CdnE03 (oDVB610/611), or Ssc-2TM (oDVB614/615).

Protein expression and purification: Ssc-CdnE03 and mutants were expressed and purified using the following approach: transformed BL21 (DE3) *E. coli* were grown in LB broth at 37°C with shaking to mid-log phase (OD_{600} 0.6-0.8), at which point the culture was cooled on ice for 10 min and induced with 0.2 mM IPTG for 16 hr at 18°C. Bacteria were harvested, resuspended in lysis buffer (25 mM Tris pH 7.4, 300 mM NaCl, 5% glycerol, 2 mM *β*-mercaptoethanol), and subjected to a single freeze-thaw cycle. The cells were incubated on ice with lysozyme, DNase I, and EDTA-free protease inhibitor cocktail. After incubating on ice for 40 min, the cells were lysed using sonication. Lysates were clarified by centrifugation and applied to cobalt affinity resin. After binding, the resin was washed extensively with lysis buffer prior to elution with lysis buffer containing 300 mM imidazole. Eluted proteins were then proteolyzed with TEV protease to remove the affinity tag during overnight 4°C dialysis to reaction buffer (25 mM HEPES-KOH pH 7.5, 250 mM KCl, 5% glycerol, 2 mM *β*-mercaptoethanol). The cleaved proteins were then passed over cobalt resin to collect the remaining tag (or uncleaved protein) and concentrated using 10,000 MWCO centrifugal filters (Amicon). Purified proteins were visualized by SDS-PAGE and used for downstream *in vitro* assays.

Nucleotide synthesis assays: Nucleotide synthesis assays were performed using a variation of the method described by Whiteley *et al.* [9]. The final reactions (50 mM CAPSO pH 9.4, 50 mM KCl, 5 mM $Mg(OAc)_2$, 1 mM DTT, 25 or 250 uM individual NTPs, trace amounts of [α-^{32}P] NTP, 5 uM nucleic acid ligand, and 5 μM enzyme) were

started with the addition of enzyme. All reactions except for those with RNA activator (2 hr) were incubated overnight at 37°C. For reactions with total RNA extracts, 500 ng was added to each condition. Reactions were stopped with the addition of 1 U of alkaline phosphatase, which removes triphosphates on the remaining NTPs and enables the visualization of cyclized nucleotide species. After a 1 hr incubation, 0.5 μL of the reaction was spotted 1.5 cm from the bottom of a PEI-cellulose thin-layer chromatography (TLC) plate, spaced 0.8 cm apart. TLC plates were developed in 1.5 M KH_2PO_4 pH 3.8 until the buffer front reached 1 cm from the top (~12 cm). The TLC plates were completely dried, covered with plastic wrap and exposed to a phosphor screen before detection by a Typhoon Trio Imager System.

To purify the Ssc-CdnE03 cyclic nucleotide product for mass spectrometry analysis, nucleotide synthesis reaction conditions were scaled up to 1 mL reactions containing 5 uM Ssc-CdnE03, 250 uM ATP, 250 uM GTP, approximately 5 ng of cabRNA, in 50 mM CAPSO pH 9.4, 50 mM KCl, 5 mM $Mg(OAc)_2$, 1 mM DTT buffer. Reactions were incubated with gentle shaking for 24 hr at 37°C followed by Quick CIP (NEB) treatment for 4 hr at 37°C. Following incubation, reactions were filtered through a 10,000 MWCO centrifugal filter (Amicon) to remove protein.

Nucleotide High Resolution Mass Spectrometry Analysis: All solvents and reagents used for chromatography were LC-MS grade. UPLC-HRMS data was acquired on a Sciex ExcionLC UPLC coupled to an X500R mass spectrometer, controlled by SCIEXOS software. Chromatography was carried out on a Phenomenex Acquity UPLC® BEH Shield RP18 (2.1 x 150 mm, 1.7 μm), under the following conditions: 3% B from 0.0 to 6.0 min, from 3% to 10% B from 6.0 to 16.0 min, 10% B until 18.0, 95% B from 18.0 to 21.0 and 3% B from 22.0 to 27.0 (A: water + 0.1% formic acid; B: acetonitrile + 0.1% formic acid) (pending of new buffer), with a flow rate of 0.25 mL/min and 1μL of injection volume. HRMS analysis were performed in positive and negative electrospray ionization mode in the range m/z 100-1200 for MS1 and MS2 scans; the maximum candidate ions subjected for Q2-MS2 experiments was 7, declustering potential of 80 V, collision energy of 5 V and temperature of 500ºC. For ESI+ HRMS experiments the spray voltage was set in 5500 V, the Q2 collision energy at 30 V with a spread of 10 V, whereas the spray voltage for ESI- HRMS was set in 4500V and the Q2 collision energy at 35 V with a spread of 10 V. The concentration of the standard solutions was 6.25 μM, and all the solutions were centrifuged (13,000 rpm x 3 min) before injection. The molecular ions for ESI modes were analyzed for all compounds, but the fragmentation in ESI- mode showed a better consistency and was consequently used for the structural analysis. The data analysis was carried out with MestReNova software (14.3.0), data output was converted with MSConvert from Proteowizard, MS2 mirror plot was obtained from GNPS using averaged MS2 spectra from GNPS molecular networking.

RNA extraction from phage infection: 10 mL of a mid-log phase *S. aureus* RN4220 culture normalized to OD_{600} 0.5 was infected with phage at MOI 10. Infection was allowed to proceed for 30 min, just before the completion of the first burst. Cells were pelleted at 4,300 x g for 5 min and flash-frozen with liquid nitrogen. The pellet was resuspended in 150 μL PBS and 50 μL lysostaphin (5 mg mL^{-1}) and incubated at 37°C for 30 min. Total RNA was extracted from *S. aureus* cells using a Direct-Zol™ RNA

MiniPrep Plus Kit (Cat. R2072). Briefly, 450 μL Trizol was added to the lysate, vigorously vortexed and centrifuged at 16,000 x g for 30 seconds. 650 μL of 100% ethanol was added to the supernatant and the samples were thoroughly vortexed. The entire volume was passed through a Zymo-Spin IIICG Column followed by in-column treatment with DNase I for 15 min at room temperature. The column was washed according to the manufacturer's protocol and RNA was eluted in 100 μL nuclease-free water.

RNA pull-down assay: His6-MBP-tagged Ssc-CdnE03 was expressed and purified as described above. Purified His6-MBP tag alone was prepared alongside as a negative control. After immobilizing ~0.2 mg of protein on cobalt resin, the column was washed extensively with lysis buffer prior to the addition of 5 mL of lysis buffer containing 1 mM $MgCl_2$, 5 units of RNaseOUT™ (ThermoFisher, Cat. 10777019), and 100 μg of total RNA extracted from cultures with or without phage infection. The RNA was incubated with the tagged Ssc-CdnE03 on the column for 40 min before washing the column with 5 volumes of lysis buffer. The column was treated with His6-tagged TEV protease to release the Ssc-CdnE03 and bound RNA. Eluted protein was collected for each sample and combined with TRI Reagent (Zymo Research, Cat. R2050-1-200). RNA was then extracted according to the Direct-Zol™ RNA MiniPrep Plus Kit (Cat. R2072) manufacturer's protocol. The final RNA product was run on a 2% agarose 1X TAE gel and stained with SyBr Gold or ethidium bromide. Eluted protein samples were collected as controls for visualization by SDS-PAGE.

RNA-sequencing: Reverse transcription of the RNA isolated from the pull-down assay was performed as detailed above. Briefly, RNA was treated with TURBO™ DNase (Thermo Fisher Scientific) before cDNA first-strand synthesis with SuperScript IV Reverse Transcriptase using random hexamers. Second-strand synthesis of the cDNA was performed with Q5 DNA polymerase at 15°C for 2 hr, followed by 75°C for 10 min in the presence of RNase H and DMSO. The cDNA was then sheared to 150-bp fragments using an S220 Covaris Focused-Ultrasonicator (peak incident power: 175 W, duty factor: 10%, cycles per burst: 200, treatment time: 430 s, temperature 4°C) in S-Series Holder microTUBEs (PN 500114). Library preparation was performed using the Illumina TruSeq Library Prep Kit. Quantification and quality check of DNA libraries were confirmed by Qubit 4.0 Fluorometer and Agilent Bioanalyzer/Tapestation, respectively. loaded to a flow cell on an Illumina MiSeq instrument (paired ends, 150 cycles). 12 pM DNA library was loaded on an Illumina MiSeq instrument for paired-end sequencing (2 x 150 cycle). Bowtie2 via the Galaxy open-source interface [43] was used to align sequencing reads to phage and host genomes. A custom Python script was used to convert the output SAM alignments into CSV files.

RNA structure prediction: RNA secondary structures were analyzed using the ViennaRNA 2.0 package [30] and visualized via the SnapGene interface.

***In vitro* transcription of cabRNA:** *In vitro* transcription (IVT) was performed according to the Thermo Scientific TranscriptAid T7 High Yield Transcription Kit protocol (Cat. K0441). Linear dsDNA for the cabRNA, host pull-down RNA, and *terS*^{S74F} phage escaper RNA sequences were PCR-amplified using oCR190/193 (sense cabRNA), oCR191/192 (antisense cabRNA), oCR194/197 (sense host RNA), oCR195/196

(antisense host RNA), and oDVB691/oCR193 (*terS*^{S74F} phage escaper RNA). The target sequence was placed downstream of a T7 promoter, which was inverted for antisense transcription reactions. For high yield *in vitro* transcription reactions, 1 μg of PCR product was combined with TranscriptAid Enzyme mix and NTPs. Following a 4 hr incubation period at 37°C, transcripts were purified according to the Direct-Zol™ RNA MiniPrep Plus Kit (Cat. R2072) manufacturer's protocol. To stimulate the re-folding and formation of a structured RNA product, the purified IVT samples were heated at 95°C for 5 min in a heat block, which was slowly cooled down to room temperature over 1 hr. Where indicated, IVT products were either heat-treated ("folded") or untreated.

Structural prediction and analysis of Ssc-CdnE03: The amino acid sequence of Ssc-CdnE03 sequence was used to seed a position-specific iterative BLAST (PSI-BLAST) search of the NCBI non-redundant protein and conserved domain databases (composition-based adjustment, E-value threshold 0.01). Putative domains identified from this search include a C-terminal "nucleotidyltransferase (NT) domain of 2'5'-oligoadenylate (2-5A) synthetase" (NT_2-5OAS) domain (Residues 61-204; E-value 2.63e-15) and an N-terminal "tRNA nucleotidyltransferase" (CCA-adding enzyme) domain (Residues 5-158; E-value 8.01e-04). A structure of the Ssc-CdnE03 was predicted using AlphaFold (ColabFold). Following structure determination, pairwise structural comparison of the rank 1 model to the full PDB database was performed using DALI. The ConSurf database was used to visualize conserved structural features of the Ssc-CdnE03. Structural alignments and generation of surface electrostatics with apo-OAS1 (PDB:4RWQ) and OAS1:dsRNA (PDB:4RWO) were performed using PyMOL.

Generation and isolation of escaper bacteriophages: Overnight cultures of *S. aureus* RN4220 were diluted 1:100 and outgrown at 37°C with shaking for 1 hr, infected with Φ80α-vir (MOI 1) for 20 min, and then treated with 1% ethyl methanesulfonate (EMS), a chemical mutagen. Cultures were allowed to lyse for 3 hr before pelleting debris and sterile-filtering the supernatant to obtain an EMS-treated mutant phage library. 100 μL of RN4220 overnight cultures harboring Ssc-CBASS were infected with a high titer mutant phage library in BHI soft agar and then plated. After incubating at 37°C overnight, individual phage plaques were picked from the top agar and resuspended in 50 μL of BHI liquid medium. Phage lysates were further purified over two rounds of passaging on RN4220 harboring Ssc-CBASS.

Whole-genome sequencing and analysis: Genomic DNA from high-titer phage stocks was extracted using a previously described method [41]. DNA was sheared to 300-bp fragments using an S220 Covaris Focused-Ultrasonicator (peak incident power: 140 W, duty factor: 10%, cycles per burst: 200, treatment time: 80 s, temperature 4°C) in S-Series Holder microTUBEs (PN 500114). Library preparation was performed using the Illumina Nextera XT DNA Library Preparation Kit protocol (Cat. FC-131-1096). 12 pM of the library was loaded on an Illumina MiSeq instrument for paired-end sequencing (2 x 150 cycle). Bowtie2 via the Galaxy open-source interface [43] was used to align sequencing reads to phage and host genomes. A custom Python script was used to convert the output SAM alignments into CSV files.

Generation of recombinant ΦNM1γ6 *terS*^{S74F} mutants: Wild-type ΦNM1γ6 was passaged on *S. aureus* RN4220 harboring Ssc-CBASS and pTerS or pTerS^{S74F} to

929 enable recombination. The infected culture supernatant was spotted onto a lawn of
930 RN4220 with *Ssc*CBASS in BHI soft agar to isolate individual escaper plaques. The *terS*
931 gene was amplified by PCR and the S74F mutation was confirmed by Sanger
932 sequencing.

933 **Phylogenetic analysis of CD-NTase sequences:** The CD-NTases from *S. schleiferi*
934 are most similar to the CdnE subtype 03 (CdnE03) described by Whiteley *et al.* [9]. All
935 CD-NTase enzymes were aligned using TCoffee Multiple Sequence Alignment tool
936 (default parameters) and used to construct a phylogenetic tree with Geneious Prime
937 using the neighbor-joining method and Jukes-Cantor genetic distance model with no
938 outgroup.

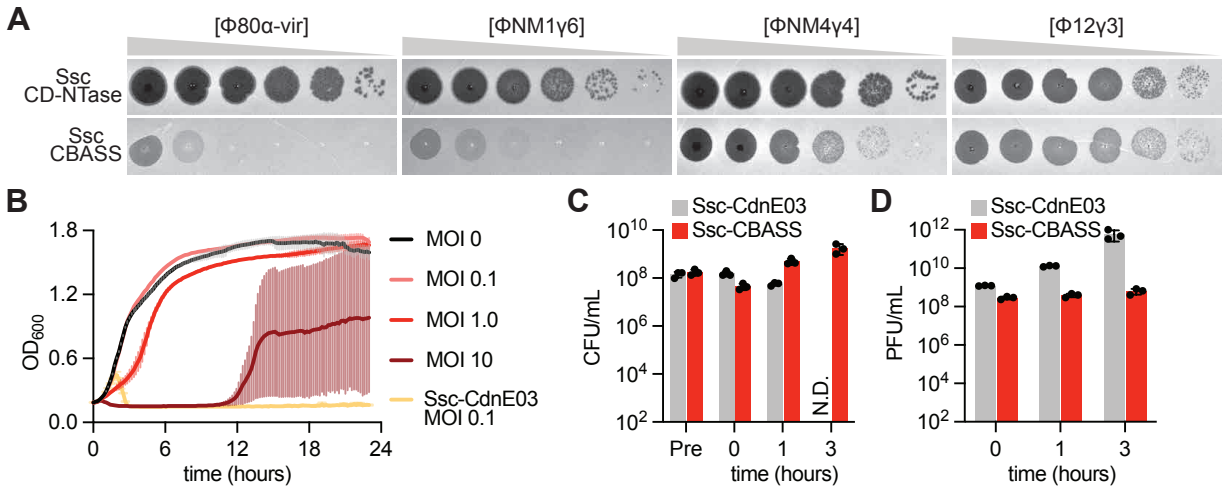

Figure 1. Banh, Roberts et al.

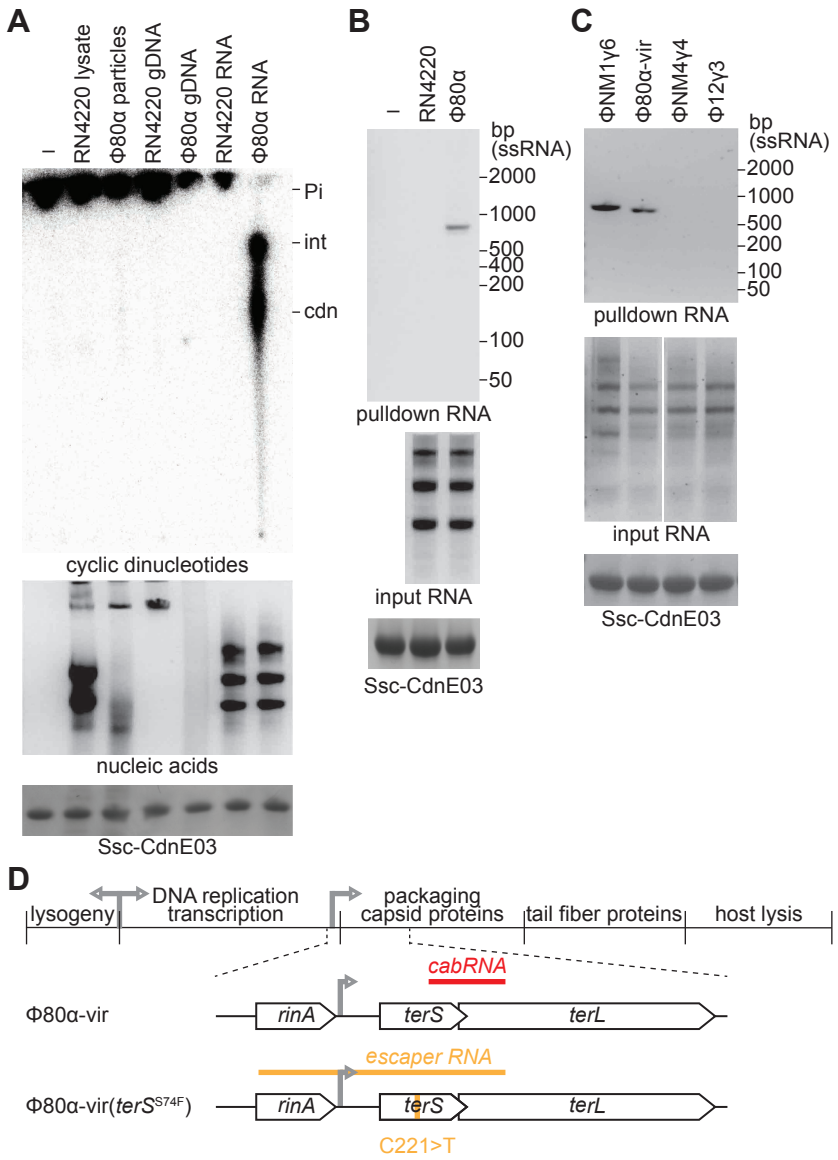

Figure 2. Banh, Roberts et al.

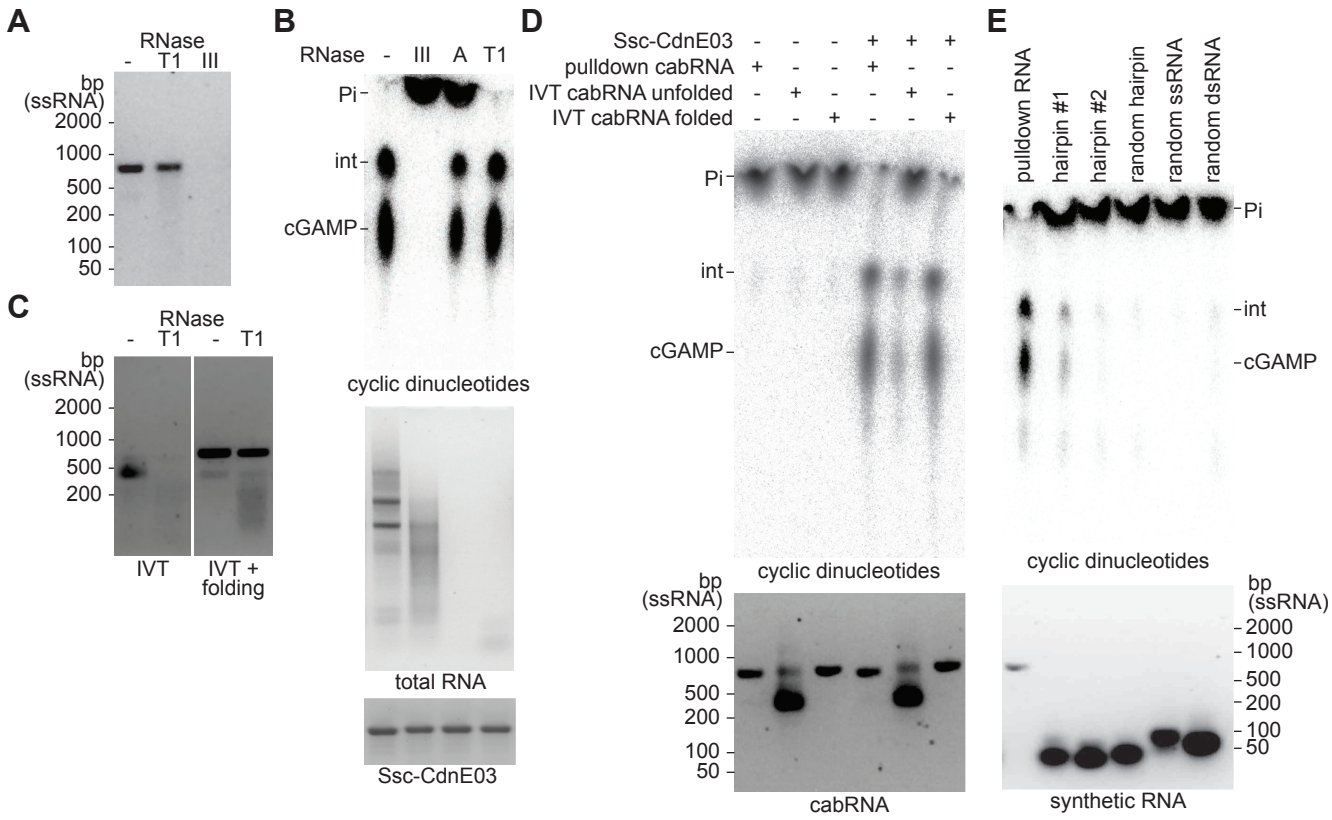

Figure 3. Banh, Roberts et al.

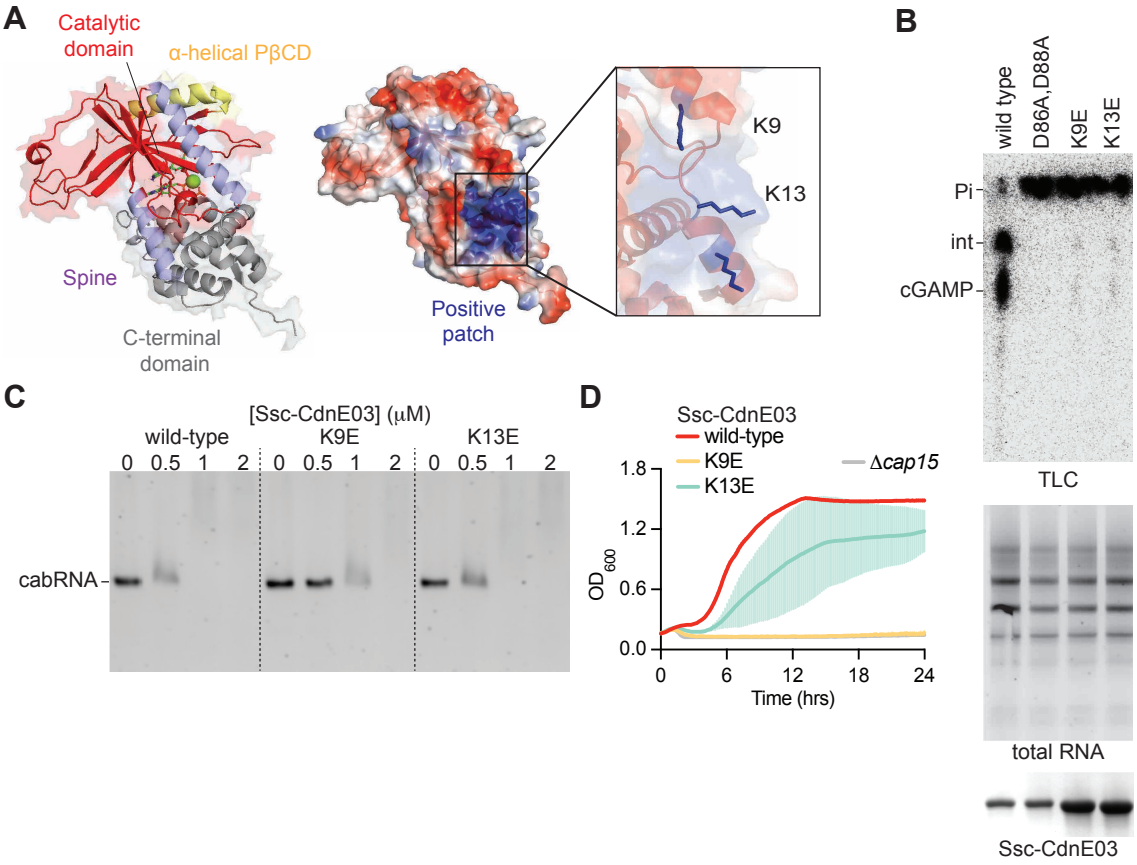

Figure 4. Banh, Roberts et al.

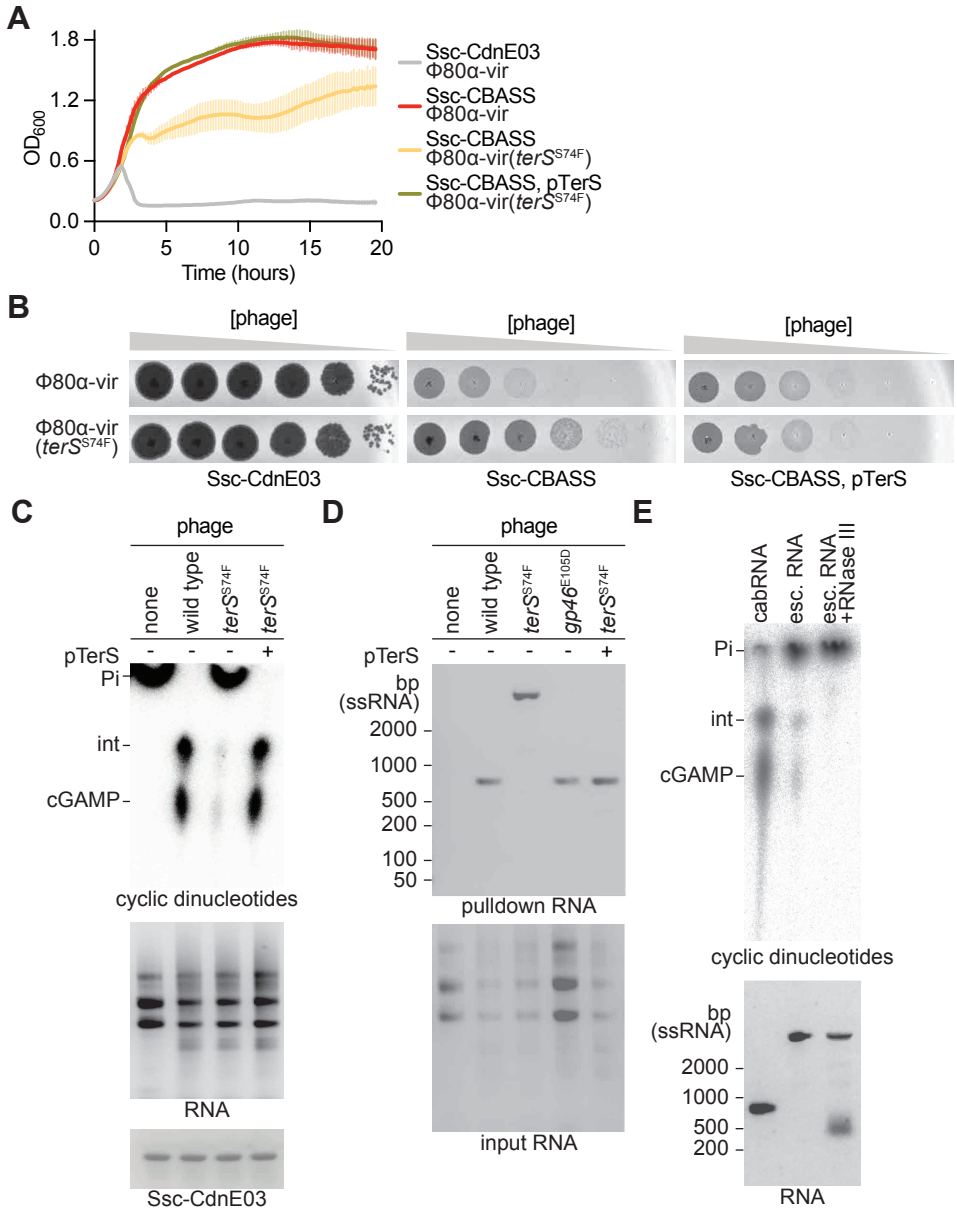

Figure 5. Banh, Roberts et al.

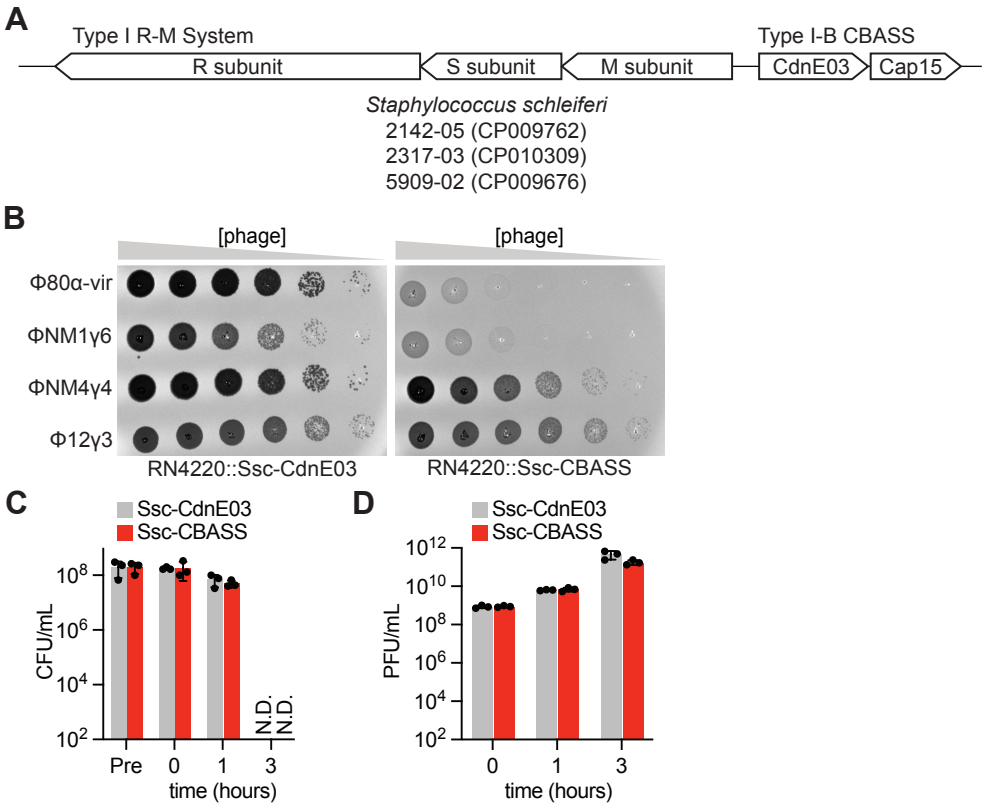

Figure S1. Banh, Roberts et al.

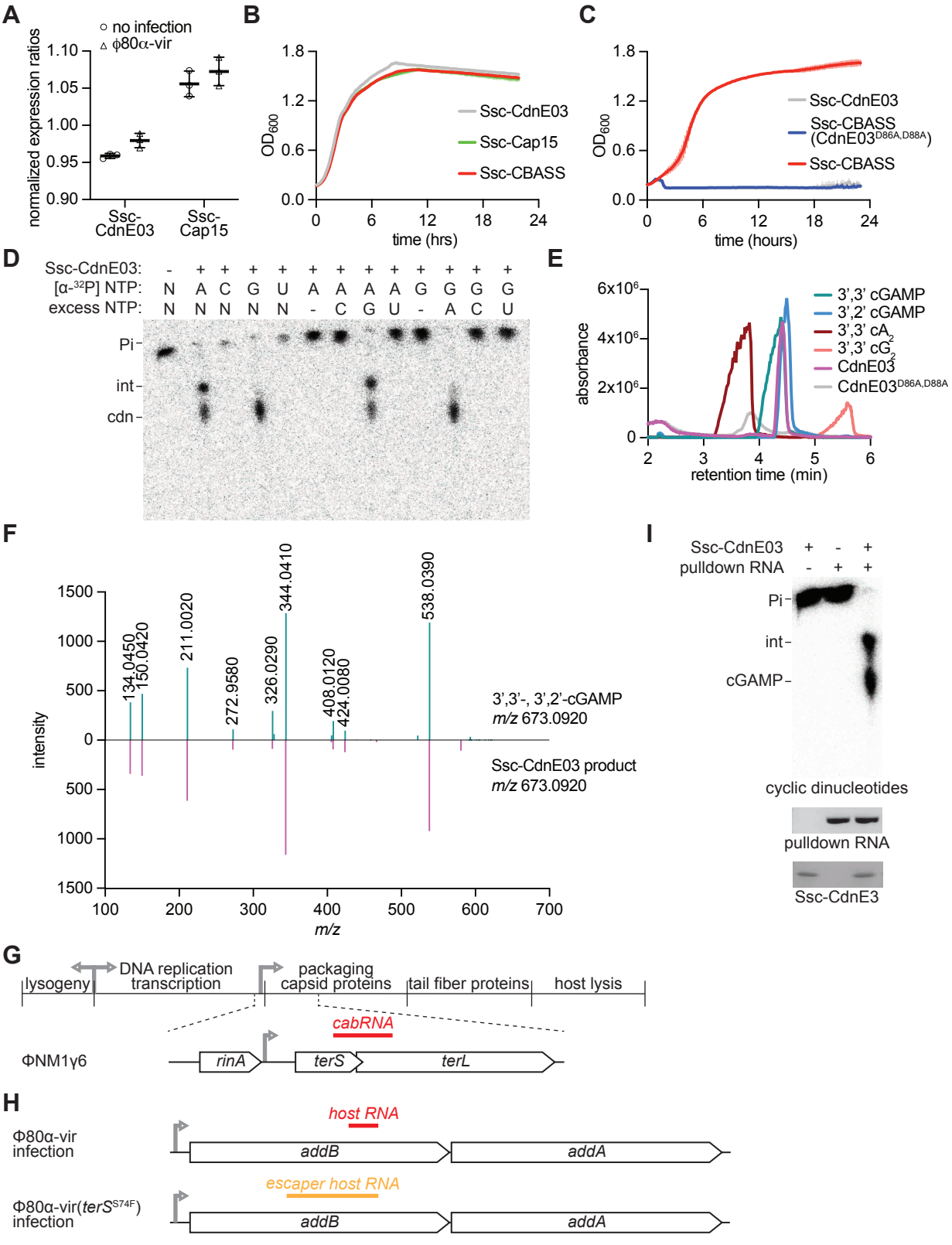

Figure S2. Banh, Roberts et al.

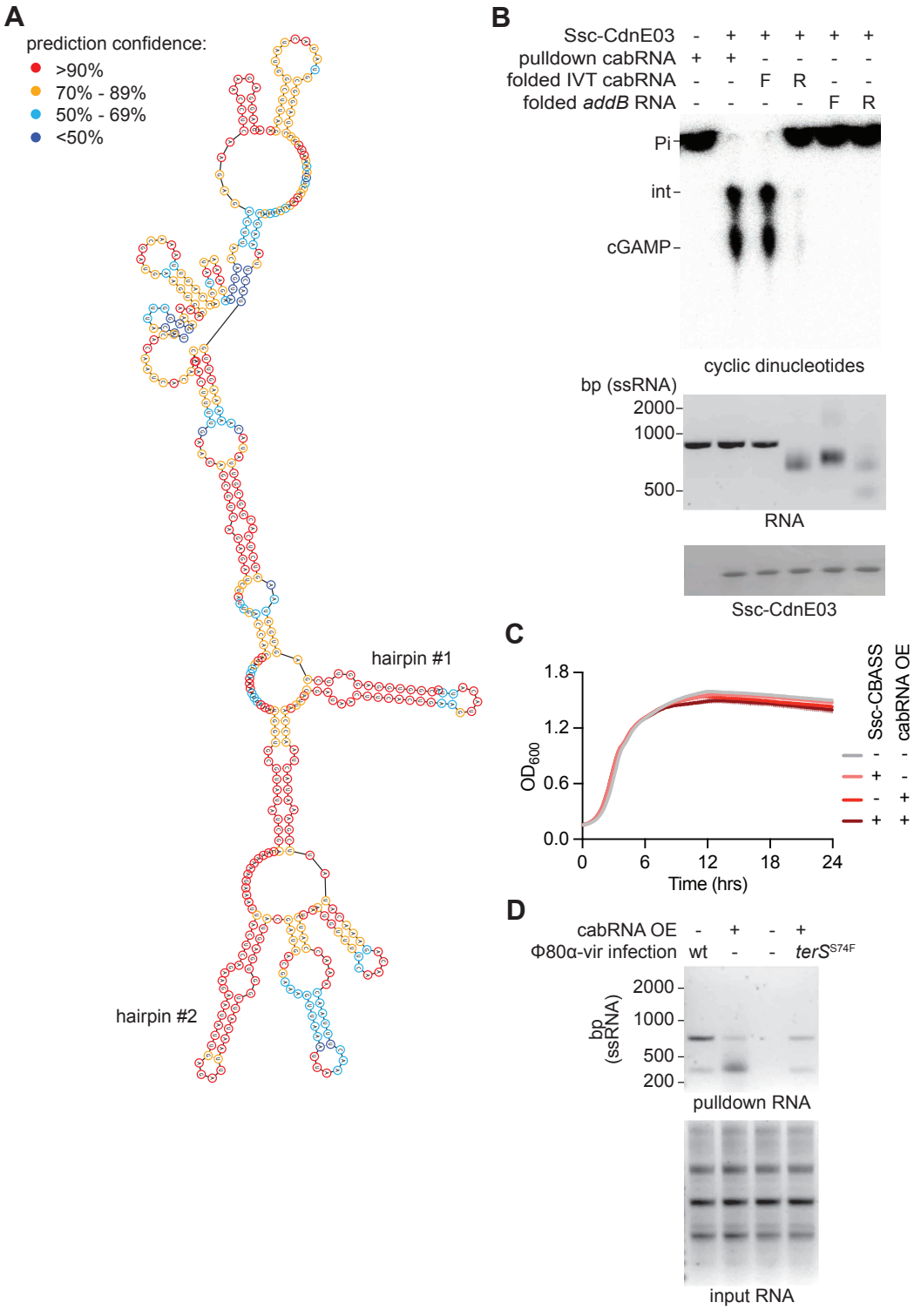

Figure S3. Bahn, Roberts et al.

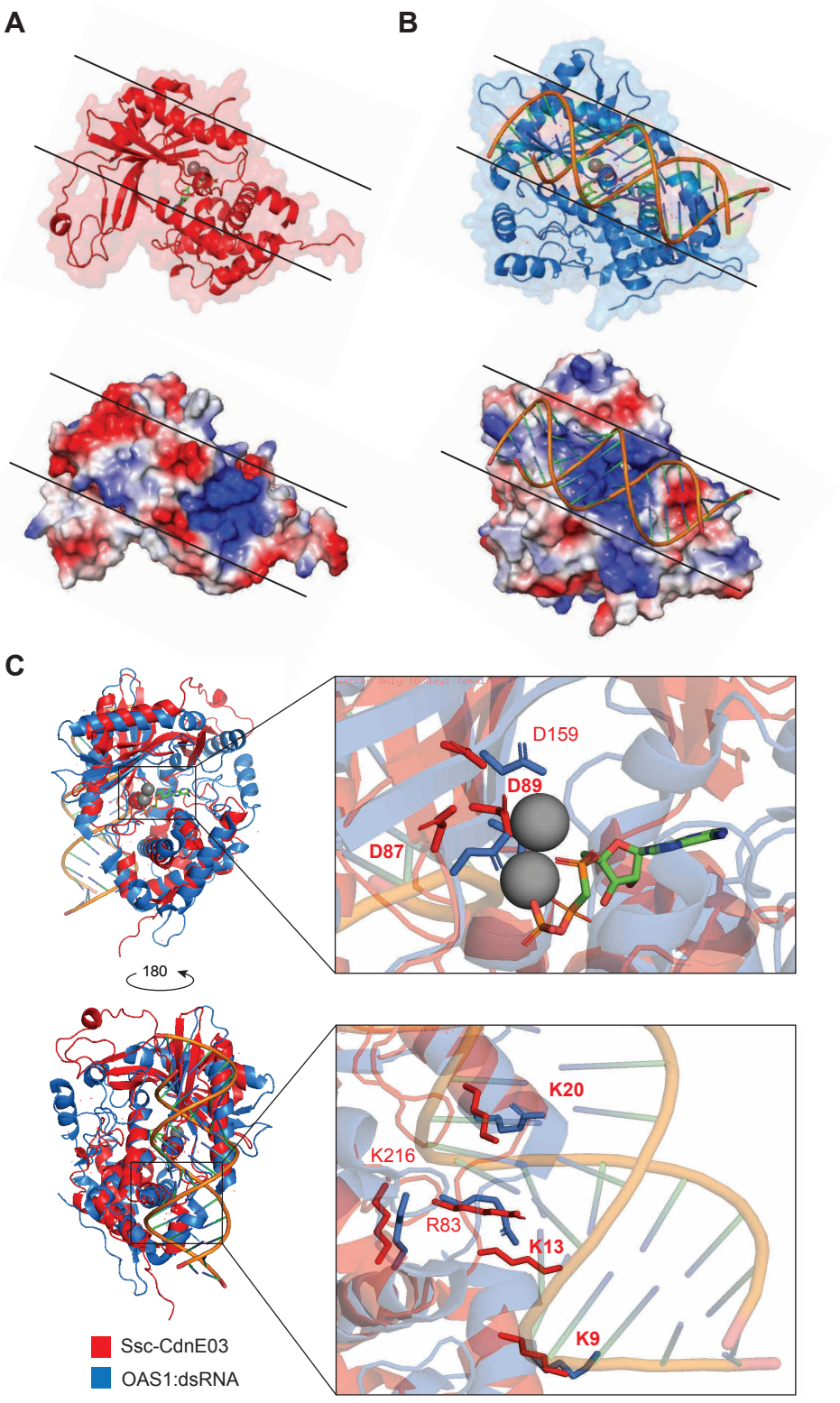

Figure S4. Banh, Roberts et al.

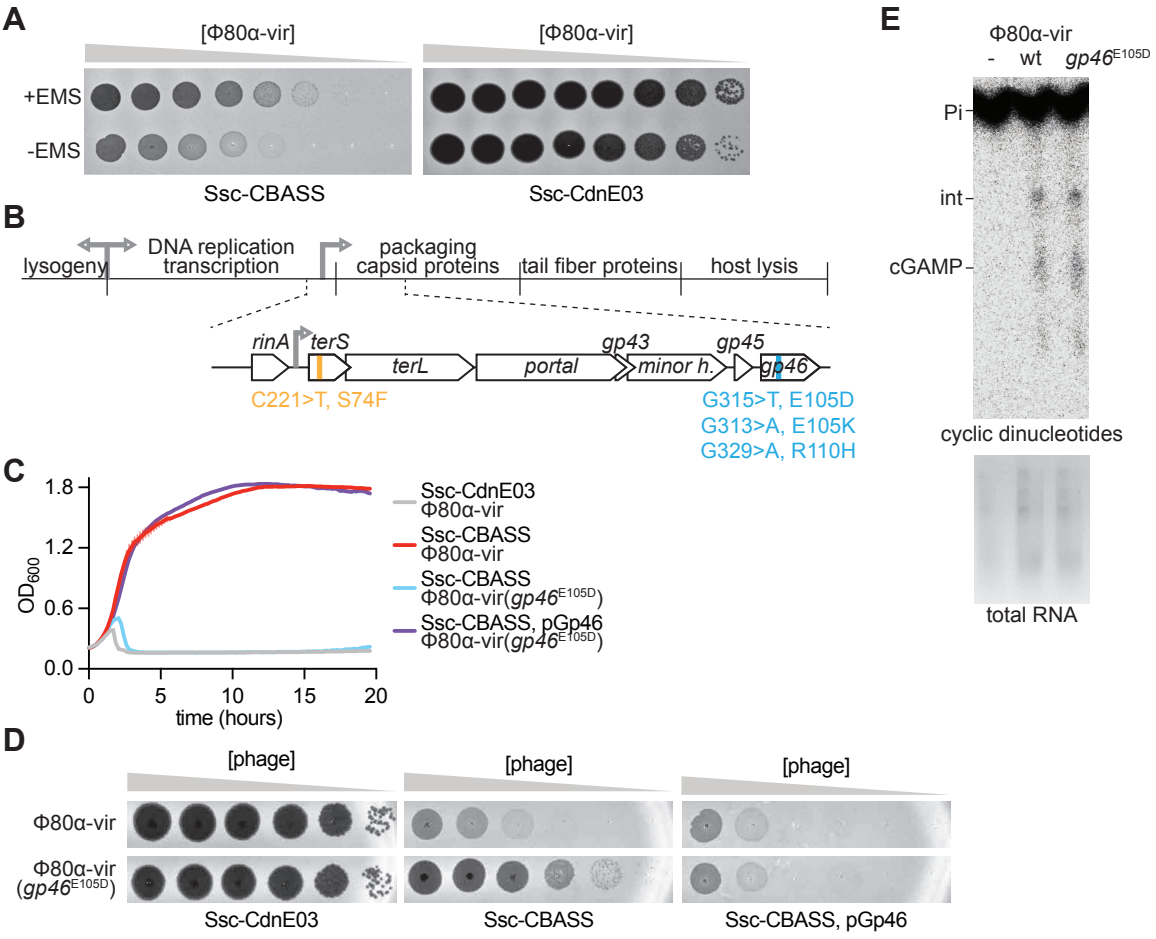

Figure S5. Banh, Roberts et al.

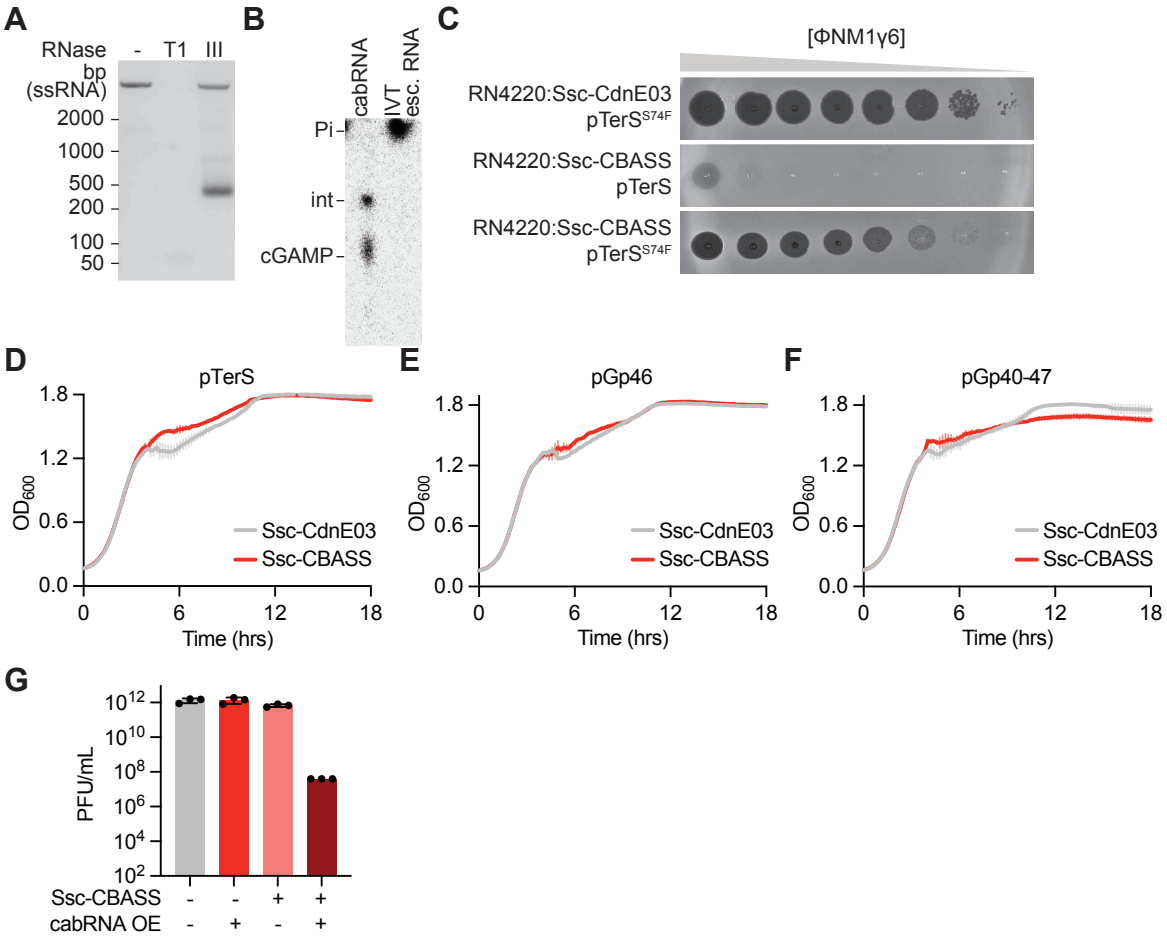

Figure S6. Banh, Roberts et al.

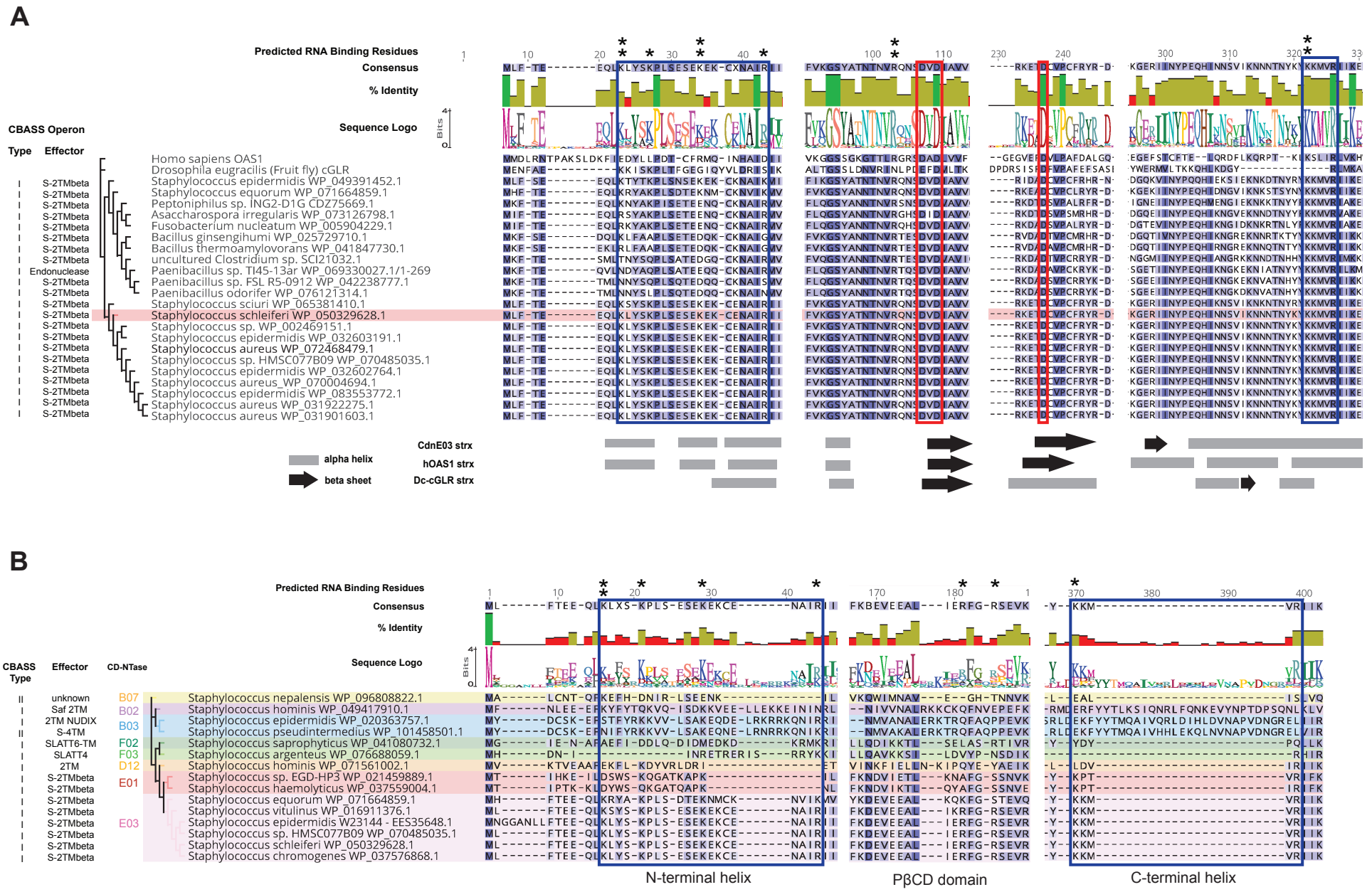
A
Predicted RNA Binding Residues
Consensus
% Identity
Sequence Logo
Bits
CBASS Operon
Type
Effector
I S-2TMbeta Homo sapiens OAS1
I S-2TMbeta Drosophila eugracilis (Fruit fly) cGLR
I S-2TMbeta Staphylococcus epidermidis WP_049391452.1
I S-2TMbeta Staphylococcus equorum WP_071664859.1
I S-2TMbeta Peptoniphilus sp. ING2-D1G CDZ75669.1
I S-2TMbeta Asaccharospora irregularis WP_073126798.1
I S-2TMbeta Fusobacterium nucleatum WP_005904229.1
I S-2TMbeta Bacillus ginsengihumi WP_025729710.1
I S-2TMbeta Bacillus thermoamylovorans WP_041847730.1
I S-2TMbeta uncultured Clostridium sp. SCI21032.1
I Endonuclease Paenibacillus sp. TI45-13ar WP_069330027.1/1-269
I S-2TMbeta Paenibacillus sp. FSL R5-0912 WP_042238777.1
I S-2TMbeta Paenibacillus odorifer WP_076121314.1
I S-2TMbeta Staphylococcus sciuri WP_065381410.1
I S-2TMbeta Staphylococcus schleiferi WP_050329628.1
I S-2TMbeta Staphylococcus sp. WP_002469151.1
I S-2TMbeta Staphylococcus epidermidis WP_032603191.1
I S-2TMbeta Staphylococcus aureus WP_072468479.1
I S-2TMbeta Staphylococcus sp. HMSC077B09 WP_070485035.1
I S-2TMbeta Staphylococcus epidermidis WP_032602764.1
I S-2TMbeta Staphylococcus aureus_WP_070004694.1
I S-2TMbeta Staphylococcus epidermidis WP_083553772.1
I S-2TMbeta Staphylococcus aureus WP_031922275.1
I S-2TMbeta Staphylococcus aureus WP_031901603.1
alpha helix
beta sheet
CdnE03 strx
hOAS1 strx
Dc-cGLR strx
B
Predicted RNA Binding Residues
Consensus
% Identity
Sequence Logo
Bits
CBASS Type
Effector
CD-NTase
II unknown B07 Staphylococcus nepalensis WP_096808822.1
I Saf 2TM B02 Staphylococcus hominis WP_049417910.1
I 2TM NUDIX B03 Staphylococcus epidermidis WP_020363757.1
II S-4TM B03 Staphylococcus pseudintermedius WP_101458501.1
I SLATT6-TM F02 Staphylococcus saprophyticus WP_041080732.1
I SLATT4 F03 Staphylococcus argenteus WP_076688059.1
I 2TM D12 Staphylococcus hominis WP_071561002.1
I S-2TMbeta E01 Staphylococcus sp. EGD-HP3 WP_021459889.1
I S-2TMbeta Staphylococcus haemolyticus WP_037559004.1
I S-2TMbeta Staphylococcus equorum WP_071664859.1
I S-2TMbeta Staphylococcus vitulinus WP_016911376.1
I S-2TMbeta E03 Staphylococcus epidermidis W23144 - EES35648.1
I S-2TMbeta Staphylococcus sp. HMSC077B09 WP_070485035.1
I S-2TMbeta Staphylococcus schleiferi WP_050329628.1
I S-2TMbeta Staphylococcus chromogenes WP_037576868.1
N-terminal helix
PβCD domain
C-terminal helix

SUPPLEMENTARY SEQUENCES FILE.

Sequences of RNA species pulled down from Ssc-CdnE03-RNA pull-down assay (related to Figures 2D and S2G-H):

400-bp bacteriophage RNA during Φ80α-vir infection (cabRNA$_{Φ80α}$): 5'-
AGAGGAGAACCUCAAGAGGCUUACAGUAAGAAAUAUGACCAUUUAAACGAUGAA
GUGGAAAAAGAGGUUACUUACACAAUCACACCAACUUUUGAAGAGCGUCAGAGA
UCUAUUGACCACAUACUAAAAGUUCAUGGUGCGUAUAUCGACAAAAAAGAAAUUA
CUCAGAAGAAUAUUGAGAUUAAUAUUGGUGAGUACGAUGACGAAAGUUAAAUUA
AACUUUAACAAACCAUCUAAUGUUUUCAACAGAAACAUAUUCGAAAUACUAACCA
AUUACGAUAACUUCACUGAAGUACAUUACGGUGGAGGUUCGAGUGGUAAGUCUC
ACGGCGUUAUACAAAAAGUUGUACUUAAAGCAUUGCAAGACUGGAAAUAUCCUA
GGCGUAUACUAUGGCUUAGA-3'

1237-bp bacteriophage RNA during Φ80α-vir *gp40*$_{S74F}$ infection: 5'-
AUGACUAAAAAGAAAUAUGGAUUAAAAUUAUCAACAGUUCGAAAGUUAGAAGAUG
AGUUGUGUGAUUAUCCUAAUUAUCAUAAGCAACUCGAAGAUUUAAGAAGUGAAA
UAAUGACACCAUGGAUUCCAACAGAUACAAAUAUAGGCGGGGAGUUUGUACCGU
CUAAUACAUCGAAAACAGAAAUGGCAGUAACUAAUUAUCUUUGUAGUAUACGAAG
AGGUAAAAUCCUUGAGUUUAAGAGCGCUAUUGAACGUAUAAUCAACACAUCAAG
UAGGAAAGAACGCGAAUUCAUUCAAGAGUAUUAUUUUAAUAAAAAGGAAUUAGU
GAAAGUUUGUGAUGACAUACACAUUUCUGAUAGAACUGCUCAUAGAAUCAAAAG
GAAAAUCAUAUCUAGAUUGGCGGAAGAGUUAGGGGAAGAGUGAAAUUGGCAGUA
AAGUGGCAGUUUUUGAUACCUAAAAUGAGAUAUUAUGAUAGUGUAGGAUAUUGA
CUAUCUUACUGCGUUUCCCUUAUCGCAAUUAGGAAUAAAGGAUCUAUGUGGGUU
GGCUGAUUAUAGCCAAUCCUUUUUUAAUUUUAAAAAGCGUAUAGCGCGAGAGUU
GGUGGUAAAUGAAAUGAACGAAAAACAAAAGAGAUUCGCAGAUGAAUAUAUAAUG
AAUGGAUGUAAUGGUAAAAAAGCAGCAAUUUCAGCAGGUUAUAGUAAGAAAACA
GCAGAGUCUUUAGCAAGUCGAUUGUUAAGAAAUGUUAAUGUUUCGGAAUAUAUU
AAAGAACGAUUAGAACAGAUACAAGAAGAGCGUUUAAUGAGCAUUACAGAAGCU
UUAGCGUUAUCUGCUU**U**UAUUGCUAGAGGAGAACCUCAAGAGGCUUACAGUAAG
AAAUAUGACCAUUUAAACGAUGAAGUGGAAAAAGAGGUUACUUACACAAUCACAC
CAACUUUUGAAGAGCGUCAGAGAUCUAUUGACCACAUACUAAAAGUUCAUGGUG
CGUAUAUCGACAAAAAAGAAAUUACUCAGAAGAAUAUUGAGAUUAAUAUUGGUGA
GUACGAUGACGAAAGUUAAAUUAAACUUUAACAAACCAUCUAAUGUUUUCAACAG
AAACAUAUUCGAAAUACUAACCAAUUACGAUAACUUCACUGAAGUACAUUACGGU
GGAGGUUCGAGUGGUAAGUCUCACGGCGUUAUACAAAAAGUUGUACUUAAAGCA
UUGCAAGACUGGAAAUAUCCUAGGCGUAUACUAUGGCUUAGA-3'

400-bp bacteriophage RNA during ΦNM1γ6 infection (cabRNA$_{ΦNM1γ6}$): 5'-
AGAGGAGAACCUCAAGAGGCUUACAGUAAGAAAUAUGACCAUUUAAACGAUGAA
GUGGAAAAAGAGGUUACUUACACAAUCACACCAACUUUUGAAGAGCGUCAGAGA
UCUAUUGACCACAUACUAAAAGUACAUGGUGCGUAUAUCGAUAAAAAAGAAAUUA
CUCAGAAGAAUAUUGAGAUUAAUAUUGGUGAGUACGAUGACGAAAGUUAAAUUA
AACUUUAACAAACCAUCUAAUGUUUUCAAUAGAAACAUAUUCGAAAUACUAACCA

AUUACGAUAACUUCACUGAAGUACAUUACGGUGGAGGUUCGAGCGGUAAGUCUC
ACGGCGUUAUACAAAAAGUUGUACUUAAAGCAUUGCAAGACUGGAAAUAUCCUA
GGCGUAUACUAUGGCUUAGA-3’

400-bp host RNA during Φ80α-vir infection: 5’-
ACAUUAACGACAACUCAAGGUAUUCCAAUUAAUAUUAGAGGGCAAAUUGACCGU
AUCGAUACGUAUACAAAGAAUGAUACAAGUUUUGUUAAUAUCAUUGACUAUAAAU
CCUCUGAAGGUAGUGCGACACUUGAUUUAACGAAAGUAUAUUAUGGUAUGCAAA
UGCAAAUGAUGACAUACAUGGAUAUCGUUUUACAAAAUAAACAACGCCUUGGAU
UAACAGAUAUUGUGAAACCAGGUGGAUUAUUAUACUUCCAUGUACAUGAACCUA
GAAUUAAAUUUAAAUCAUGGUCUGAUAUUGAUGAAGAUAAACUAGAACAAGAUUU
AAUUAAAAAGUUUAAGUUGAGUGGUUUAGUUAAUGCAGACCAAACUGUUAUUGA
UGCAUUGGAUAUUCGUUUAG-3’

1237-bp host RNA during Φ80α-vir (*gp40*$_{S74F}$) infection: 5’-
CAGAUGGAUGAAGCAUUUGUUUGUUAUGUUGCUAUGACUAGAGCUAAGGGAGA
UGUUACAUUUUCUUACAGUCUAAUGGGAUCAAGUGGUGAUGAUAAGGAGAUCAG
CCCAUUUUUAAAUCAAAUUCAAUCAUUGUUCAACCAAUUGGAAAUUACUAACAUU
CCUCAAUACCAUGAAGUUAACCCAUUGUCACUAAUGCAACAUGCUAAGCAAACCA
AAAUUACAUUAUUUGAAGCAUUGCGUGCUUGGUUAUAUGAUGAAAUUGUGGCUG
AUAGUUGGUUAGAUGCUUAUCAAGUAAUUAGAGAUAGCGAUCAUUUAAAUCAAG
GUUUAGAUUAUUUAAUGUCAGCAUUAACGUUUGACAAUGAAACUGUAAAAUUAG
GUGAAACGUUGUCUAAAGAUUUAUAUGGUAAGGAAAUCAAUGCCAGUGUAUCCC
GUUUUGAAGGUUAUCAACAAUGCCCAUUUAAACACUAUGCGUCACAUGGUCUGA
AACUAAAUGAGCGAACGAAGUAUGAACUUCAAAACUUUGAUUUAGGUGAUAUUU
UCCAUUCUGUUUUAAAAUAUAUAUCUGAACGUAUUAAUGGCGAUUUUAAACAAU
UAGACCUGAAAAAAAUAAGACAAUUAACGAAUGAAGCAUUGGAAGAAAUUUUACC
UAAAGUUCAGUUUAAUUUAUUAAAUUCUUCAGCUUACUAUCGUUAUUUAUCAAG
ACGCAUUGGCGCUAUUGUAGAAACAACACUAAGCGCAUUAAAAUAUCAAGGCAC
GUAUUCAAAGUUUAUGCCAAAACAUUUUGAGACAAGUUUUAGAAGGAAACCAAG
AACAAAUGACGAAUUAAUUGCACAAACAUUAACGACAACUCAAGGUAUUCCAAUU
AAUAUUAGAGGGCAAAUUGACCGUAUCGAUACGUAUACAAAGAAUGAUACAAGU
UUUGUUAAUAUCAUUGACUAUAAAUCCUCUGAAGGUAGUGCGACACUUGAUUUA
ACGAAAGUAUAUUAUGGUAUGCAAAUGCAAAUGAUGACAUACAUGGAUAUCGUU
UUACAAAAUAAACAACGCCUUGGAUUAACAGAUAUUGUGAAACCAGGUGGAUUA
UUAUACUUCCAUGUACAUGAACCUAGAAUUAAAUUUAAAUCAUGGUCUGAUAUU
GAUGAAGAUAAACUAGAACAAGAUUUAAUUAAAAAGUUUAAGUUGAGUGGUUUA
GUUAAUGCAGACCAAACUGUUAUUGAUGCAUUGGAUAUUCGUUUAG-3’

Sequences of *gp40* from bacteriophages used in this study:

***gp40* sequence from Φ80α-vir:** 5'-
ATGAACGAAAAACAAAAGAGATTCGCAGATGAATATATAATGAATGGATGTAATGGT
AAAAAAGCAGCAATTTCAGCAGGTTATAGTAAGAAAACAGCAGAGTCTTTAGCAAG
TCGATTGTTAAGAAATGTTAATGTTTCGGAATATATTAAAGAACGATTAGAACAGAT
ACAAGAAGAGCGTTTAATGAGCATTACAGAAGCTTTAGCGTTATCTGCTTCTATTGC
TAGAGGAGAACCTCAAGAGGCTTACAGTAAGAAATATGACCATTTAAACGATGAAG
TGGAAAAAGAGGTTACTTACACAATCACACCAACTTTTGAAGAGCGTCAGAGATCT
ATTGACCACATACTAAAAGTTCATGGTGCGTATATCGACAAAAAAGAAATTACTCAG
AAGAATATTGAGATTAATATTGGTGAGTACGATGACGAAAGTTAA-3'

***gp40* sequence from Φ80α-vir *gp40*$_{S74F}$:** 5'-
ATGAACGAAAAACAAAAGAGATTCGCAGATGAATATATAATGAATGGATGTAATGGT
AAAAAAGCAGCAATTTCAGCAGGTTATAGTAAGAAAACAGCAGAGTCTTTAGCAAG
TCGATTGTTAAGAAATGTTAATGTTTCGGAATATATTAAAGAACGATTAGAACAGAT
ACAAGAAGAGCGTTTAATGAGCATTACAGAAGCTTTAGCGTTATCTGCTT**T**TATTGC
TAGAGGAGAACCTCAAGAGGCTTACAGTAAGAAATATGACCATTTAAACGATGAAG
TGGAAAAAGAGGTTACTTACACAATCACACCAACTTTTGAAGAGCGTCAGAGATCT
ATTGACCACATACTAAAAGTTCATGGTGCGTATATCGACAAAAAAGAAATTACTCAG
AAGAATATTGAGATTAATATTGGTGAGTACGATGACGAAAGTTAA-3'

***gp40* sequence from ΦNM1γ6:** 5'-
ATGAACGAAAAACAAAAGAGATTCGCAGATGAATATATAATGAATGGATGTAATGGT
AAAAAAGCAGCAATTACAGCAGGTTATAGTAAGAAAACAGCAGAGTCTTTAGCAAG
TCGATTGTTAAGAAATGTTAATGTTTCGGAATATATTAAAGAACGATTAGAACAGAT
ACAAGAAGAGCGTTTAATGAGTATTACAGAAGCTTTAGCGTTATCTGCTTCTATTGC
TAGAGGAGAACCTCAAGAGGCTTACAGTAAGAAATATGACCATTTAAACGATGAAG
TGGAAAAAGAGGTTACTTACACAATCACACCAACTTTTGAAGAGCGTCAGAGATCT
ATTGACCACATACTAAAAGTACATGGTGCGTATATCGATAAAAAAGAAATTACTCAG
AAGAATATTGAGATTAATATTGGTGAGTACGATGACGAAAGTTAA-3'

***gp40* sequence from ΦNM1γ6 *gp40*$_{S74F}$ recombinant:** 5'-
ATGAACGAAAAACAAAAGAGATTCGCAGATGAATATATAATGAATGGATGTAATGGT
AAAAAAGCAGCAATTTCAGCAGGTTATAGTAAGAAAACAGCAGAGTCTTTAGCAAG
TCGATTGTTAAGAAATGTTAATGTTTCGGAATATATTAAAGAACGATTAGAACAGAT
ACAAGAAGAGCGTTTAATGAGCATTACAGAAGCTTTAGCGTTATCTGCTT**T**TATTGC
TAGAGGAGAACCTCAAGAGGCTTACAGTAAGAAATATGACCATTTAAACGATGAAG
TGGAAAAAGAGGTTACTTACACAATCACACCAACTTTTGAAGAGCGTCAGAGATCT
ATTGACCACATACTAAAAGTTCATGGTGCGTATATCGACAAAAAAGAAATTACTCAG
AAGAATATTGAGATTAATATTGGTGAGTACGATGACGAAAGTTAA-3'

SUPPLEMENTARY TABLES.

Table S1. Bacterial strains used in this study:

Species	Strain	Genotype	Origin
S. aureus	RN4220	Wild type	Kreiswerth et al., Nature (1983)
S. aureus	RN4220	::Ssc-CdnE03-cmR	Chromosomal integration (see Methods)
S. aureus	RN4220	::Ssc-CBASS-cmR	Chromosomal integration (see Methods)
E. coli	BL21 (DE3)	F^- *ompT gal dcm lon hsdS*$_B$ ($r_B^- m_B^-$)	Thermo Fisher Scientific

Table S2. Phages used in this study:

Phage	Host	Genotype	Origin
Φ80α-vir	*S. aureus*	Wild type	This study; strictly lytic mutant of Φ80α isolated from type III CRISPR-Cas targeting of *cI* repressor gene
Φ80α-vir	*S. aureus*	*terS* S74F (C221>T)	This study; isolated from EMS chemical mutagenesis screen for Ssc-CBASS escapers
Φ80α-vir	*S. aureus*	*gp46* E105D (G315>T)	This study; isolated from EMS chemical mutagenesis screen for Ssc-CBASS escapers
Φ80α-vir	*S. aureus*	*gp46* E105K (G313>A)	This study; isolated from EMS chemical mutagenesis screen for Ssc-CBASS escapers
Φ80α-vir	*S. aureus*	*gp46* R110H (G329>A)	This study; isolated from EMS chemical mutagenesis screen for Ssc-CBASS escapers
ΦNM1γ6	*S. aureus*	Wild type	Goldberg et al., Nature (2014)
ΦNM1γ6	*S. aureus*	Φ80α *terS* S74F	This study; isolated through recombination with Φ80α-vir $terS^{S74F}$
ΦNM4γ4	*S. aureus*	Wild type	Heler et al., Nature (2015)
Φ12γ3	*S. aureus*	Wild type	Modell et al., Nature (2017)

Table S3. Plasmids used in this study:

Plasmid	Description	Source	Construction Notes
pDVB08	*S. epidermidis* RP62a type III-A CRISPR-Cas system with programmed spacer targeting Φ80α *cI* gene	This study	Ligation of BsaI-digested pGG78 and annealed oDVB16/oDVB17
pDVB301	Ssc-CdnE03 (cyclase only) with native promoter on pC194-based vector	This study	Gibson Assembly: oDVB401+oDVB402 (pDVB47 template), oDVB405+oDVB406 (*S. schleiferi* 2142-05 genomic DNA template)
pDVB302	Ssc-Cap15 (effector only) with native promoter on pC194-based vector	This study	Gibson Assembly: oDVB401+oDVB402 (pDVB47 template), oDVB407+oDVB408 (*S. schleiferi* 2142-05 genomic DNA template)
pDVB303	Ssc-CBASS (full system) with native promoter on pC194-based vector	This study	Gibson Assembly: oDVB401+oDVB402 (pDVB47 template), oDVB405+oDVB408 (*S. schleiferi* 2142-05 genomic DNA template)
pDVB313	Ssc-CBASS with native promoter and catalytically inactive Ssc-CdnE03 (D86A, D88A mutation) on pC194-based vector	This study	Gibson Assembly: oDVB459+oDVB460 (pDVB303 template)
pDVB317	His6-MBP Ssc-CdnE03 on IPTG-inducible pET-based vector for recombinant protein expression	This study	Gibson Assembly: oDVB479+oDVB480 (pET His6 MBP TEV LIC cloning vector template), oDVB481+oDVB482 (*S. schleiferi* 2142-05 genomic DNA template)
pDVB318	His6-MBP Ssc-CdnE03 (D86A, D88A mutation) on IPTG-inducible pET-based vector for recombinant protein expression	This study	Gibson Assembly: oDVB459+oDVB460 (pDVB317 template)
pDVB374	Φ80α *gp46* on IPTG-inducible pE194-based vector with strong RBS (also denoted as “pGp46”)	This study	Gibson Assembly: oCR95+oCR96 (pPM134 template), oDVB624+oDVB625 (Φ80α-vir genomic DNA template)

pDVB377	Φ80α *terS* on IPTG-inducible pE194-based vector with strong RBS (also denoted "pTerS")	This study	Gibson Assembly: oCR95+oCR96 (pPM134 template), oDVB628+oDVB629 (Φ80α-vir genomic DNA template)
pDVB377 (*terS*^{S74F})	Φ80α *terS* S74F on IPTG-inducible pE194-based vector with strong RBS (also denoted "pTerS^{S74F}")	This study	Gibson Assembly: oCR95+oCR96 (pPM134 template), oDVB628+oDVB629 (Φ80α-vir *terS*^{S74F} genomic DNA template)
pDVB378	Φ80α *gp40-gp47* on IPTG-inducible pE194-based vector with strong RBS	This study	Gibson Assembly: oCR95+oCR96 (pPM134 template), oDVB626+oDVB628 (Φ80α-vir genomic DNA template)
pDVB392	Ssc-CBASS with native promoter and Ssc-CdnE03 (K9E mutation) on pC194-based vector	This study	Gibson Assembly: oDVB56+oDVB695 (pDVB303 template), oDVB57+oDVB696 (pDVB303 template)
pDVB393	Ssc-CBASS with native promoter and Ssc-CdnE03 (K13E mutation) on pC194-based vector	This study	Gibson Assembly: oDVB56+oDVB697 (pDVB303 template), oDVB57+oDVB698 (pDVB303 template)
pDVB396	His6-MBP Ssc-CdnE03 (K9E mutation) on IPTG-inducible pET-based vector for recombinant protein expression	This study	Gibson Assembly: oDVB695+oDVB705 (pDVB317 template), oDVB696+oDVB706 (pDVB317 template)
pDVB397	His6-MBP Ssc-CdnE03 (K13E mutation) on IPTG-inducible pET-based vector for recombinant protein expression	This study	Gibson Assembly: oDVB697+oDVB705 (pDVB317 template), oDVB698+oDVB706 (pDVB317 template)
pDVB400	400-bp cabRNA from Φ80α-vir (sense direction) on aTc-inducible pE194-based vector with terminators	This study	Gibson Assembly: oDVB461+oDVB462 (pJTR162 template), oDVB679+oDVB680 (Φ80α-vir genomic DNA template)
pDVB401	400-bp RNA from Φ80α-vir (antisense direction) on aTc-inducible pE194-based vector with terminators	This study	Gibson Assembly: oDVB461+oDVB462 (pJTR162 template), oDVB681+oDVB682 (Φ80α-vir genomic DNA template)
pDVB404	400-bp RNA from RN4220 (sense direction) on aTc-	This study	Gibson Assembly: oDVB461+oDVB462 (pJTR162 template), oDVB685+oDVB686

	inducible pE194-based vector with terminators		*S. aureus* RN4220 genomic DNA template)
pDVB405	400-bp RNA from RN4220 (antisense direction) on aTc-inducible pE194-based vector with terminators	This study	Gibson Assembly: oDVB461+oDVB462 (pJTR162 template), oDVB687+oDVB688 (*S. aureus* RN4220 genomic DNA template)
pCR35	Ssc-CdnE03 (cyclase only) on IPTG-inducible pE194-based vector	This study	Gibson Assembly: oCR95+oCR96 (pPM134 template), oCR98+oCR100 (*S. schleiferi* 2142-05 genomic DNA template)
pCR36	Ssc-CBASS (full system) on IPTG-inducible pE194-based vector	This study	Gibson Assembly: oCR95+oCR96 (pPM134 template), oCR99+oCR100 (*S. schleiferi* 2142-05 genomic DNA template)
pCR37	Ssc-Cap15 (effector only) on IPTG-inducible pE194-based vector	This study	Gibson Assembly: oCR95+oCR96 (pPM134 template), oCR99+oCR111 (*S. schleiferi* 2142-05 genomic DNA template)

Table S4. Oligonucleotide primers used in this study:

Primer	Sequence
oDVB16	GAACATTGCTCGTTTGCATAGTTAAGCACATTTTG
oDVB17	CGATCAAAATGTGCTTAACTATGCAAACGAGCAAT
oDVB401	CAAACGAAAATTGGATAAAGTGGGA
oDVB402	TCGTTTGTTGAACTAATGGGTGCTT
oDVB405	AAGCACCCATTAGTTCAACAAACGAGACTTTTCTTGTGATTTTCTTTGCGAAAAATATTG
oDVB406	TCCCACTTTATCCAATTTTCGTTTGTCATTCATATTTTTTCTCACCACTATATTCAAAAT
oDVB407	AAGCACCCATTAGTTCAACAAACGATAGATGTAAAGAATTATTTTGAATATAGTGGTGAG
oDVB408	TCCCACTTTATCCAATTTTCGTTTGAAGCTTATCATAAATGATGTGGTTTTTGATAAGGT
oDVB426	GCGCCTTCACGAATTTGTTC
oDVB427	CACCGTTCTGGTTCGAGTTT
oDVB459	CACTGCAATTGCAACTGCACTATTTTGTCTTACATTGGTATTTGTTGCATACG
oDVB460	CAAAATAGTGCAGTTGCAATTGCAGTGGTAAAAGAAAGTGAGTTTTTTGATAAATAT
oDVB461	CTCCTAGGTCATTTGATATGCCTCCGGATATCACTCTATCAATGATAGAGAGCTTATTTT
oDVB462	CTAGATAAACCTTCAGACGTACATACATTTACTCCTAAATACCATAAATTAGCTGAGGCG
oDVB479	GGATTGGAAGTACAGGTTTTCCTCGATCCCATTAGTCTGCGCGTCTTTCAGGGCTTCATC
oDVB480	GATCCGGCTGCTAACAAAGCCCGAAAGGAAGCTGAGTTGGCTGCTGCCCACCGCTGAGCAA
oDVB481	GGGATCGAGGAAAACCTGTACTTCCAATCCTTGTTATTTACTGAAGAACAATTAAAATTA
oDVB482	TTCCTTTCGGGCTTTGTTAGCAGCCGGATCTCATTCATATTTTTTCTCACCACTATATTC
oDVB565	GGTGTTGAAACGCGATACTTTTCTAATAATGATAGCGAACTATTGAAGAGTCACATGTTTTATTGGAGTGGACTTTTCTTGTGATTTTCT
oDVB566	GCTAATTGACAAGGTCTCATAAATGACTCAGCAAACGATTGCAATGTATTGATACGGTTATTCTGTTTATTTATAAAAGCCAGTCATTAG
oDVB610	TGTTTCTAGTAATAAGCCTCCGTATC
oDVB611	CCTCTTCTTACCTCACTTCTTCC
oDVB614	TCATGTACGGTATGGCAAATAGG
oDVB615	ACAATTTCCACTTCCACATAAACC
oDVB624	TTAAGCTTGTACTTAGGAGGATGATTATTTATGGAAGAAAATAAACTTAAGTTTAATTTG

oDVB625	CCGATTGCAGTATAAATTTAACGATCACTCTTAATTTTTAATAATTCTTTTTTGTCTAGC
oDVB626	CCGATTGCAGTATAAATTTAACGATCACTCTTAAACTTCTCCTGGAACTGAATCTGTTCT
oDVB628	TTAAGCTTGTACTTAGGAGGATGATTATTTATGAACGAAAAACAAAAGAGATTCGCAGAT
oDVB629	CCGATTGCAGTATAAATTTAACGATCACTCTTAACTTTCGTCATCGTACTCACCAATATT
oDVB679	TATCCGGAGGCATATCAAATGACCTAGGAGAGAGGAGAACCTCAAGAGGCTTACAGTAAG
oDVB680	AAATGTATGTACGTCTGAAGGTTTATCTAGTCTAAGCCATAGTATACGCCTAGGATATTT
oDVB681	AAATGTATGTACGTCTGAAGGTTTATCTAGAGAGGAGAACCTCAAGAGGCTTACAGTAAG
oDVB682	TATCCGGAGGCATATCAAATGACCTAGGAGTCTAAGCCATAGTATACGCCTAGGATATTT
oDVB685	TATCCGGAGGCATATCAAATGACCTAGGAGACATTAACGACAACTCAAGGTATTCCAATT
oDVB686	AAATGTATGTACGTCTGAAGGTTTATCTAGCTAAACGAATATCCAATGCATCAATAACAG
oDVB687	AAATGTATGTACGTCTGAAGGTTTATCTAGACATTAACGACAACTCAAGGTATTCCAATT
oDVB688	TATCCGGAGGCATATCAAATGACCTAGGAGCTAAACGAATATCCAATGCATCAATAACAG
oDVB691	TAATACGACTCACTATAATGACTAAAAAGAAATATGG
oDVB695	CTGAAGAACAATTAGAATTATATTCTAAACCATTGTCAGAATCTGAAAAAGAAAA
oDVB696	TTCTGACAATGGTTTAGAATATAATTCTAATTGTTCTTCAGTAAATAACAA
oDVB697	ACAATTAAAATTATATTCTGAACCATTGTCAGAATCTGAAAAAGAAAAGT
oDVB698	ATTCTGACAATGGTTCAGAATATAATTTTAATTGTTCTTCAGTAAATAACAA
oDVB705	TTGCATTCGATTCCTGTTTGTAATTGTCC
oDVB706	GGACAATTACAAACAGGAATCGAATGCAA
oCR95	AAATAATCATCCTCCTAAGTACAAGCTTAATTGTTATCCGCTCACAATTCCACACATTAT
oCR96	GAGTGATCGTTAAATTTATACTGCAATCGGATGCGATTATTGAATAAAAGATATGAGAGA
oCR98	CCGATTGCAGTATAAATTTAACGATCACTCTCATTCATATTTTTTCTCACCACTATATTC
oCR99	CCGATTGCAGTATAAATTTAACGATCACTCTTATTTTAGTTTTTTGAGTCTTAGATCACC
oCR100	TTAAGCTTGTACTTAGGAGGATGATTATTTTTGTTATTTACTGAAGAACAATTAAAATTA

oCR111	TTAAGCTTGTACTTAGGAGGATGATTATTTATGAATGACAAAATAAAT CATTTGATTAAA
oCR190	TAATACGACTCACTATAAGAGGAGAACCTCAAGAGGC
oCR191	TAATACGACTCACTATATCTAAGCCATAGTATACGCCTAGG
oCR192	AGAGGAGAACCTCAAGAGGC
oCR193	TCTAAGCCATAGTATACGCCTAGG
oCR194	TAATACGACTCACTATAACATTAACGACAACTCAAGG
oCR195	TAATACGACTCACTATACTAAACGAATATCCAATGCAT
oCR196	ACATTAACGACAACTCAAGG
oCR197	CTAAACGAATATCCAATGCAT

Table S5. RNA oligonucleotides used in this study:

RNA oligo	Sequence	Description
oCR114	GCUAAACAAACAGCAAUAGAGUA CGUACAAGGCUUCUCUACAAAA	Random 45bp hairpin-forming ssRNA for *in vitro* nucleotide synthesis assays
oCR150	AAUAAACAAACAGCAAUAGAGUA CGUACAAGGCUUGUCUACAAAA	ssRNA for *in vitro* nucleotide synthesis assays
oCR151	UUUUGUAGACAAGCCUUGUACGU ACUCUAUUGCUGUUUGUUUAUU	dsRNA for *in vitro* nucleotide synthesis assays; sequence of the bottom strand is displayed
oCR198	UACGAUAACUUCACUGAAGUACA UUACGGUGGAGGUUCGAG	ssRNA hairpin #1 from Φ80α-vir cabRNA for *in vitro* nucleotide synthesis assays
oCR199	AUUACUCAGAAGAAUAUUGAGAU UAAUAUUGGUGAGUACG	ssRNA hairpin #2 from Φ80α-vir cabRNA for *in vitro* nucleotide synthesis assays

Supplementary Text.

High Resolution Mass Spectrometry Analysis of Ssc-CdnE03 reaction products.

The Full HRMS of the products of the Ssc-CdnE03 cyclase shows that this peak corresponds to a compound identified from its mono and double charged ions in the positive and negative ionization modes, that allow the molecular formula $C_{15}H_{19}N_5O_{13}P_2$ to be predicted, consistent with the molecular formula of cGAMP.

MS^2 experiments were run in both ionization modes, however, the negative shows more diagnostic fragments and a consistent fragmentation pattern throughout the set of evaluated ions. The MS^2 spectra of both cGAMP isomers show identical fragmentation to the Ssc-CdnE03 product, being particularly relevant the presence of fragment ions from cleavages a (a1, a2), b (b1, b2) and c (c1, c2) that allow identifying this product as a dimeric nucleotide constituted by GMP and AMP units. Based on these results we conclude that the Ssc-CdnE03 product is a cGAMP isomer or a mixture of them.

NEGATIVE ION MODE ACQUISITION

Characterization of standard 3´,3´-cGAMP:

- Full HRMS (-ESI):

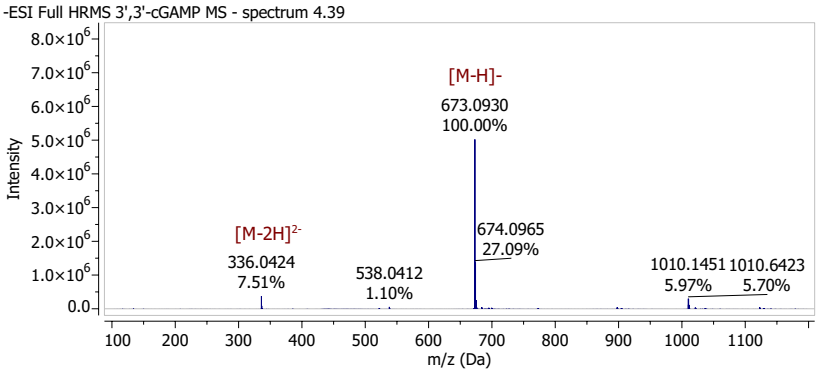

Ion	Formula	*m/z* obs.	*m/z* theo.	RDB	Δppm
$[M-H]^-$	$C_{20}H_{23}N_{10}O_{13}P_2^-$	673.0930	673.0926	13.5	0.59
$[M-2H]^{2-}$	$C_{20}H_{22}N_{10}O_{13}P_2^{2-}$	336.0424	336.0427	14.0	-0.89

- MS/MS

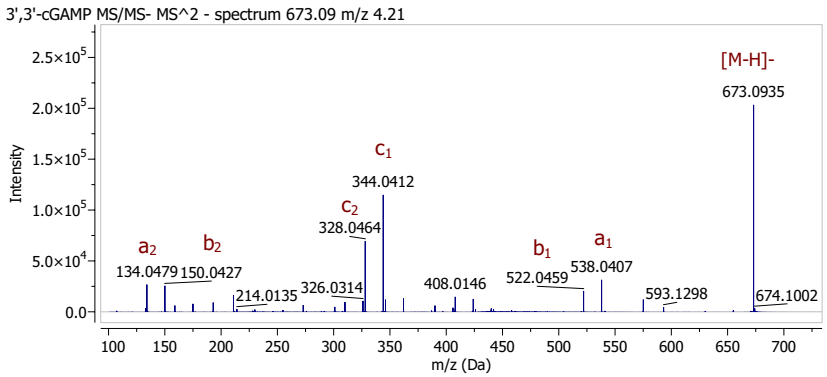

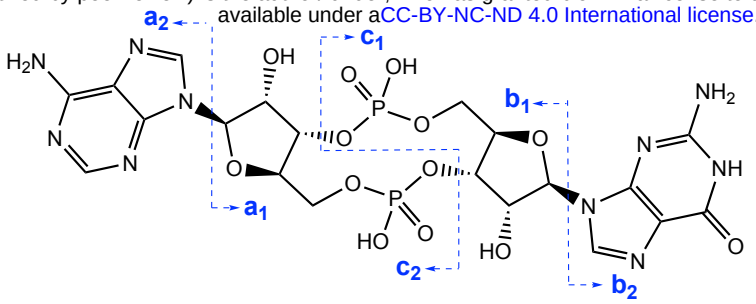

Chemical Formula: $C_{20}H_{24}N_{10}O_{13}P_2$
Exact Mass: 674.10

Cleavage	Ion	Formula	*m/z* obs.	*m/z* theo.	RDB	Δppm
a	a_1, $[X-H]^-$	$C_{15}H_{18}N_5O_{13}P_2^-$	538.0407	538.0382	8.5	4.64
	a_2, $[X-H]^-$	$C_5H_4N_5^-$	134.0479	134.0472	6.5	5.23
b	b_1, $[X-H]^-$	$C_{15}H_{18}N_5O_{12}P_2^-$	522.0459	522.0433	8.5	4.98
	b_2, $[X-H]^-$	$C_5H_4N_5O^-$	150.0427	150.0421	6.5	4.00
c	c_1, $[X-H]^-$	$C_{10}H_{11}N_5O_7P^-$	344.0412	344.0402	7.5	2.91
	c_2, $[X-H]^-$	$C_{10}H_{11}N_5O_6P^-$	328.0464	328.0452	7.5	3.65

Characterization of standard 3´,2´-cGAMP:

- Full HRMS (-ESI):

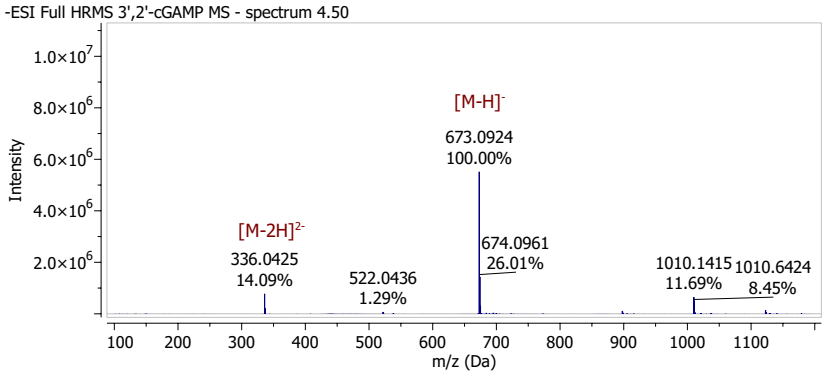

Ion	Formula	*m/z* obs.	*m/z* theo.	RDB	Δppm
$[M-H]^-$	$C_{20}H_{23}N_{10}O_{13}P_2^-$	673.0924	673.0916	13.5	1.20
$[M-2H]^{2-}$	$C_{20}H_{22}N_{10}O_{13}P_2^-$	336.0425	336.0427	14.0	-0.59

- MS/MS:

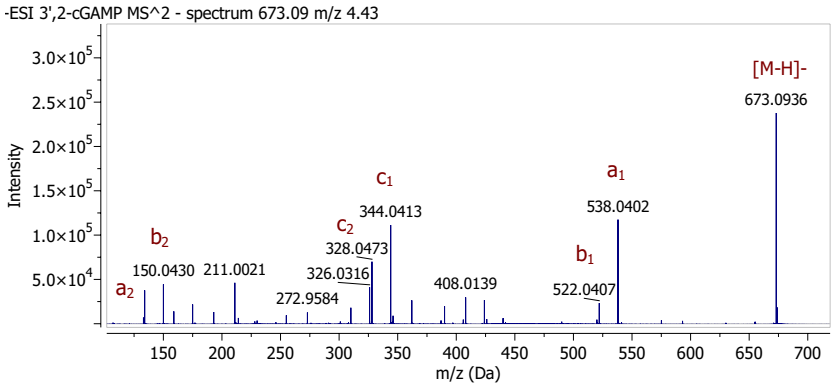

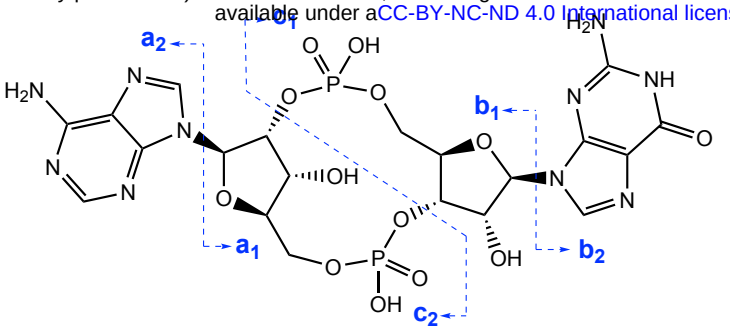

Chemical Formula: $C_{20}H_{24}N_{10}O_{13}P_2$
Exact Mass: 674.10

Cleavage	Ion	Formula	*m/z* obs.	*m/z* theo.	RDB	Δppm
a	a_1, $[X-H]^-$	$C_{15}H_{18}N_5O_{13}P_2^-$	538.0402	538.0382	8.5	3.71
	a_2, $[X-H]^-$	$C_5H_4N_5^-$	134.0482	134.0472	6.5	7.46
b	b_1, $[X-H]^-$	$C_{15}H_{18}N_5O_{12}P_2^-$	522.0407	522.0433	8.5	-4.86
	b_2, $[X-H]^-$	$C_5H_4N_5O^-$	150.0430	150.0421	6.5	5.77
c	c_1, $[X-H]^-$	$C_{10}H_{11}N_5O_7P^-$	344.0413	344.0402	7.5	3.39
	c_2, $[X-H]^-$	$C_{10}H_{11}N_5O_6P^-$	328.0473	328.0452	7.5	6.32

Characterization of standard 3´,3´-cyclic-dAMP:

- Full HRMS (-ESI):

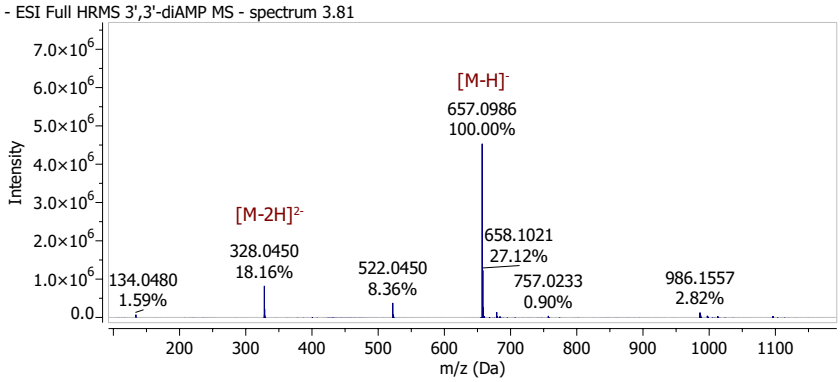

Ion	Formula	*m/z* obs.	*m/z* theo.	RDB	Δppm
$[M-H]^-$	$C_{20}H_{23}N_{10}O_{12}P_2^-$	657.0986	657.0978	13.5	1.21
$[M-2H]^{2-}$	$C_{20}H_{22}N_{10}O_{13}P_2^{2-}$	328.0450	328.0452	14.0	-0.61

- MS/MS

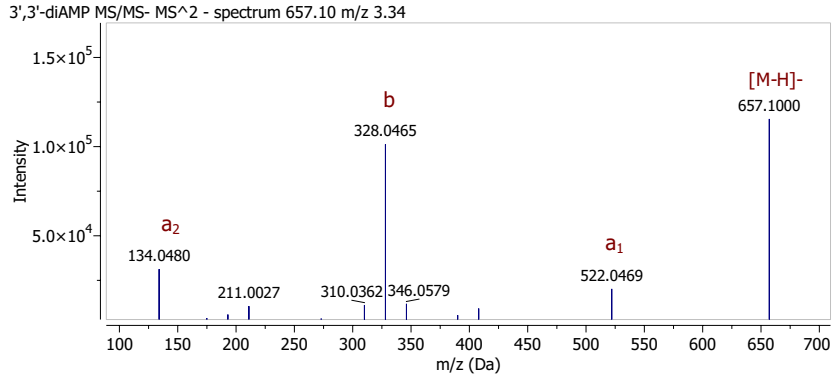

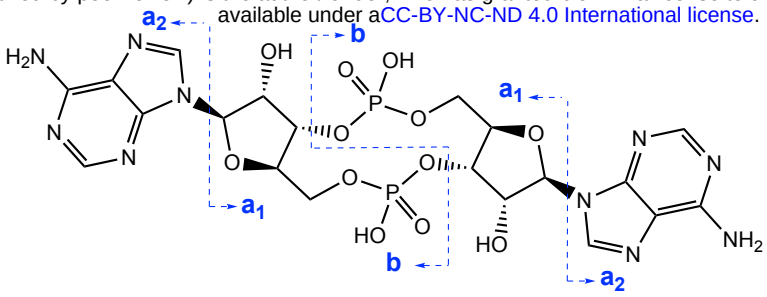

Chemical Formula: $C_{20}H_{24}N_{10}O_{12}P_2$
Exact Mass: 658.11

Cleavage	Ion	Formula	*m/z* obs.	*m/z* theo.	RDB	Δppm
a	a_1, $[X-H]^-$	$C_{15}H_{18}N_5O_{12}P_2^-$	522.0469	522.0433	8.5	6.89
	a_2, $[X-H]^-$	$C_5H_4N_5^-$	134.0480	134.0472	6.5	5.97
b	b $[X-H]^-$	$C_{10}H_{11}N_5O_6P^-$	328.0465	328.0452	7.5	3.94

Characterization of standard 3´,3´-cyclic-dGMP:

- Full HRMS (-ESI):

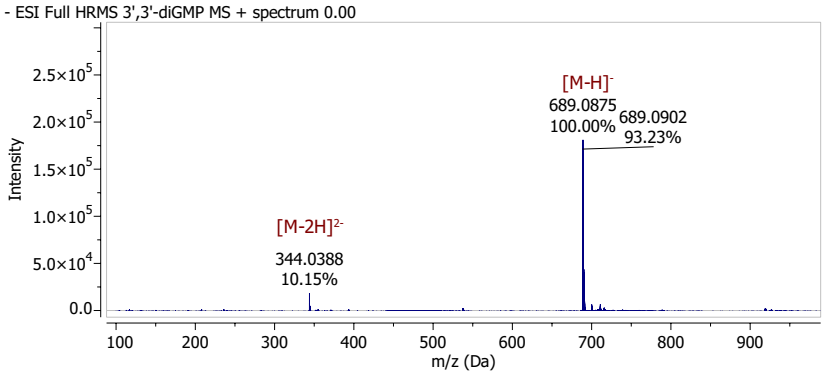

Ion	Formula	*m/z* obs.	*m/z* theo.	RDB	Δppm
$[M-H]^-$	$C_{20}H_{23}N_{10}O_{14}P_2^-$	689.0875	689.0876	13.5	-0.14
$[M-2H]^{2-}$	$C_{20}H_{22}N_{10}O_{14}P_2^{2-}$	344.0388	344.0402	14.0	-4.07

- MS/MS

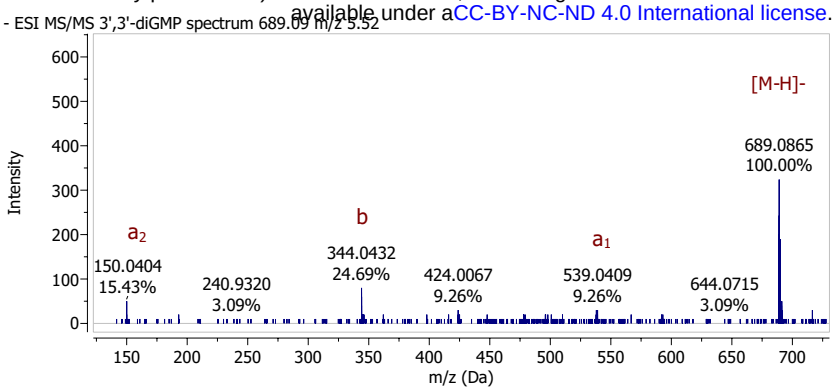

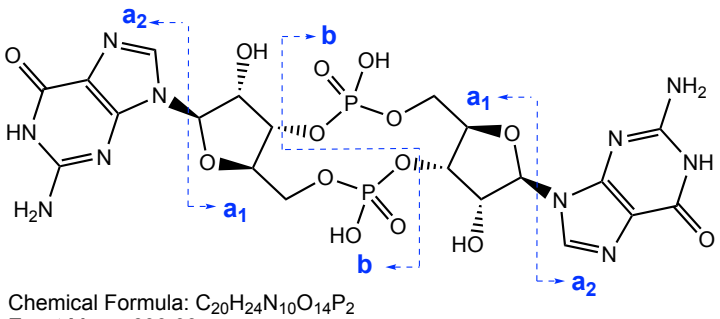

Chemical Formula: $C_{20}H_{24}N_{10}O_{14}P_2$
Exact Mass: 690,09

Cleavage	Ion	Formula	*m/z* obs.	*m/z* theo.	RDB	Δppm
a	a_1, $[X-H]^-$	$C_{15}H_{18}N_5O_{12}P_2^-$	538.0367	538.0382	8.5	-2.71
	a_2, $[X-H]^-$	$C_5H_4N_5O^-$	150.0416	150.0421	6.5	-3.24
b	b $[X-H]^-$	$C_{10}H_{11}N_5O_7P^-$	344.0394	344.0402	7.5	-2.28

Analysis of WT enzyme product:

- Full HRMS (-ESI):

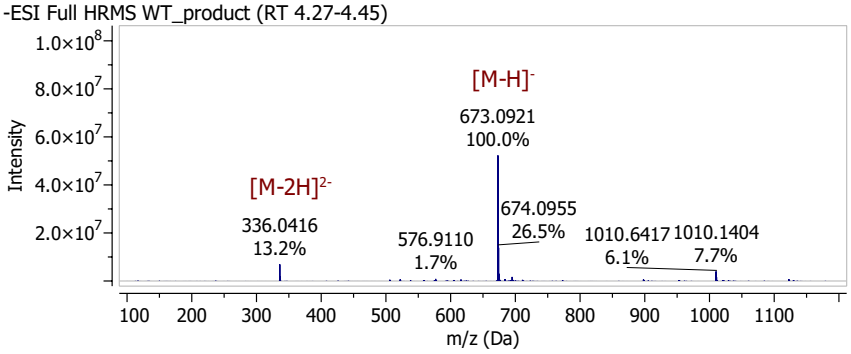

Ion	Formula	*m/z* obs.	*m/z* theo.	RDB	Δppm
$[M-H]^-$	$C_{20}H_{23}N_{10}O_{13}P_2^-$	673.0921	673.0916	13.5	0.74
$[M-2H]^{2-}$	$C_{20}H_{22}N_{10}O_{13}P_2^{2-}$	336.0416	336.0427	14.0	-3.27

- MS/MS

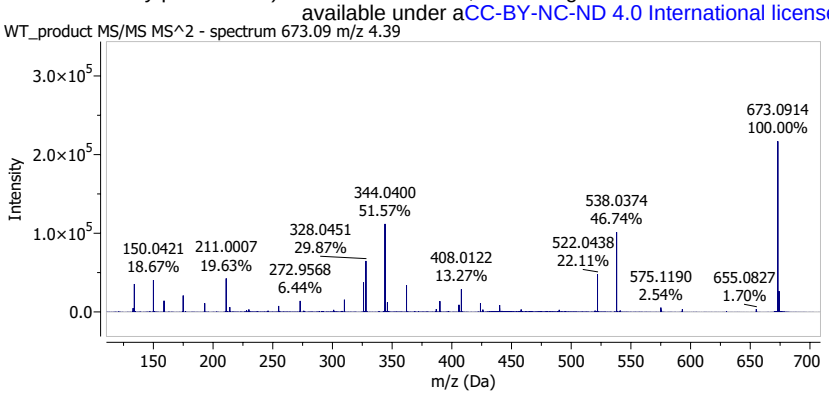

Ion	Formula	*m/z* obs.	*m/z* theo.	RDB	Δppm
$[X-H]^-$	$C_{15}H_{18}N_5O_{13}P_2^-$	538.0374	538.0382	8.5	-1.38
$[X-H]^-$	$C_{15}H_{18}N_5O_{12}P_2^-$	522.0438	522.0433	8.5	1.09
$[X-H]^-$	$C_{10}H_{11}N_5O_7P^-$	344.0400	344.0402	7.5	-0.39
$[X-H]^-$	$C_{10}H_{11}N_5O_6P^-$	328.0451	328.0452	7.5	-0.45
$[X-H]^-$	$C_5H_4N_5O^-$	150.0421	150.0421	6.5	-0.23
$[X-H]^-$	$C_5H_4N_5^-$	134.0471	134.0472	6.5	-0.75

POSITIVE ION MODE ACQUISITION

Characterization of standard 3´,2´-cGAMP:

- Full HRMS (+ESI):

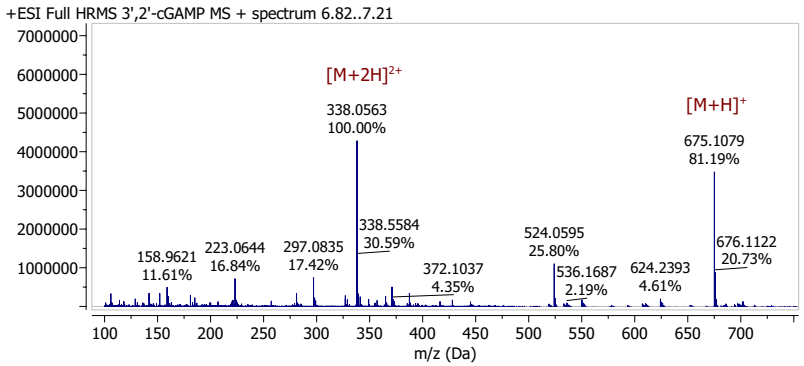

Ion	Formula	*m/z* obs.	*m/z* theo.	RDB	Δppm
$[M+H]^+$	$C_{20}H_{25}N_{10}O_{13}P_2^+$	675.1079	675.1072	12.5	0.99
$[M+2H]^{2+}$	$C_{20}H_{26}N_{10}O_{13}P_2^{2+}$	338.0562	338.0572	12.0	-2.95

Characterization of standard 3´,3´-cGAMP:

- Full HRMS (+ESI):

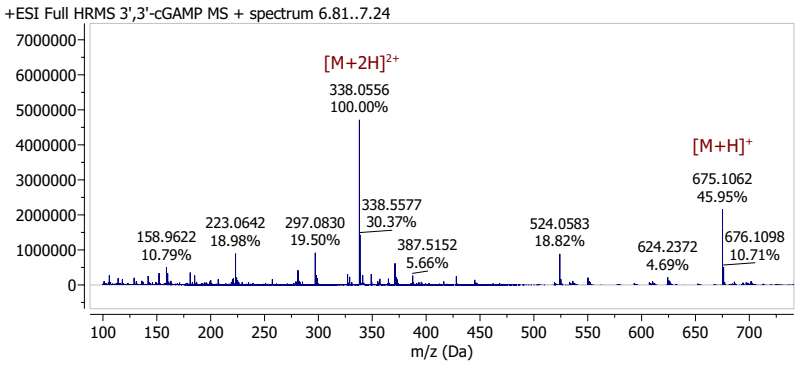

Ion	Formula	*m/z* obs.	*m/z* theo.	RDB	Δppm
$[M+H]^+$	$C_{20}H_{25}N_{10}O_{13}P_2^+$	675.1062	675.1072	12.5	-1.48
$[M+2H]^{2+}$	$C_{20}H_{26}N_{10}O_{13}P_2^{2+}$	338.0556	338.0572	12.0	-4.73

Characterization of standard 3´,3´-cyclic-dAMP:

- Full HRMS (+ESI):

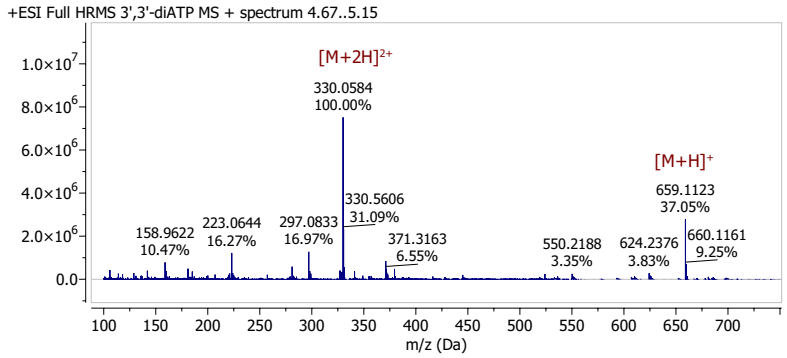

Ion	Formula	*m/z* obs.	*m/z* theo.	RDB	Δppm
$[M+H]^+$	$C_{20}H_{25}N_{10}O_{12}P_2^+$	659.1123	659.1123	12.5	-0.05
$[M+2H]^{2+}$	$C_{20}H_{26}N_{10}O_{12}P_2^{2+}$	330.0584	330.0598	12.0	-4.24

Characterization of standard 3´,3´-cyclic-dGMP:

- Full HRMS (+ESI):

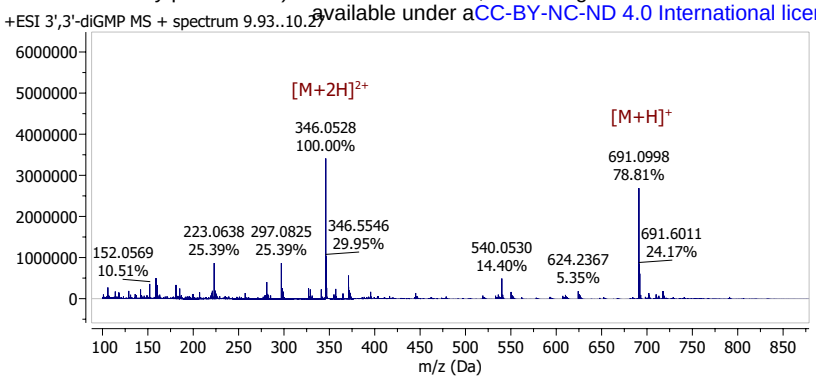

Ion	Formula	*m/z* obs.	*m/z* theo.	RDB	Δppm
$[M+H]^+$	$C_{20}H_{25}N_{10}O_{14}P_2^+$	691.0998	691.1021	12.5	-3.32
$[M+2H]^{2+}$	$C_{20}H_{26}N_{10}O_{14}P_2^{2+}$	346.0528	346.0547	12.0	-5.49

Analysis of WT enzyme product:

- Full HRMS (+ESI):

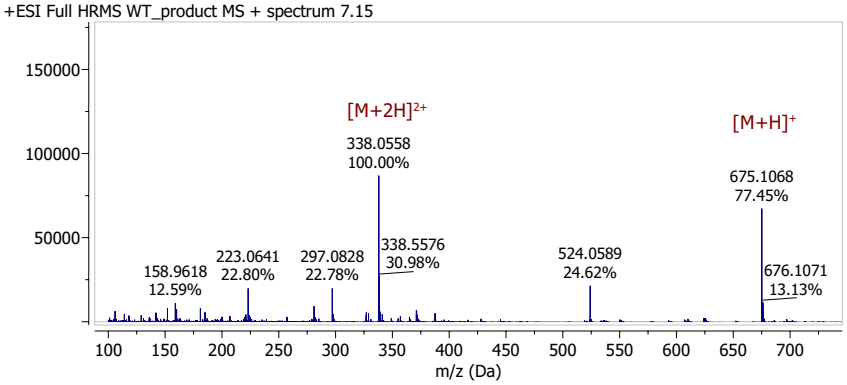

Ion	Formula	*m/z* obs.	*m/z* theo.	RDB	Δppm
$[M+H]^+$	$C_{20}H_{25}N_{10}O_{13}P_2^+$	675.1068	675.1072	12.5	-0.59
$[M+2H]^{2+}$	$C_{20}H_{26}N_{10}O_{13}P_2^{2+}$	338.0557	338.0572	12.0	-4.43